Journal of Civil Structural Health Monitoring (2023) 13:873–899
https://doi.org/10.1007/s13349-022-00633-w

ORIGINAL PAPER

Prestressed concrete bridge tested to failure: the Alveo Vecchio viaduct case study

D. Tonelli[1] · F. Rossi[2] · F. Brighenti[1] · A. Verzobio[1] · A. Bonelli[1] · D. Zonta[1]

Received: 31 March 2022 / Accepted: 8 September 2022 / Published online: 7 October 2022

Abstract

The number of bridges approaching or exceeding their initial design life has been increasing dramatically. Meanwhile, bridges are withstanding an ever-increasing traffic volume, both in number and weight of vehicles. Analytical and numerical models can predict bridges' response to traffic loads and their ultimate capacity with low uncertainties; however, such uncertainties increase as bridges age due to deterioration mechanisms. Non-destructive tests of material specimens and full-scale load tests allow for updating structural models and predicting bridges' responses with higher accuracy. On-site load tests with different load levels provide different information on the bridge behaviour (e.g., elastic response, first-crack load, and ultimate capacity), which impact the model updating differently. This paper compares the observed response of the Alveo Vecchio viaduct, a prestressed concrete (PC) bridge subjected to a controlled load test up to its failure, with its predicted response provided by four structural models. The observed response is measured by an extensive structural health monitoring system, while the structural models are developed with different levels of refinement and uncertainty in the input parameters. This study gives an insight into the ultimate load-carrying capacity of existing PC bridges and their behaviour during a whole load test to failure. The results show that the load-carry capacity of the Alveo Vecchio viaduct is almost four times higher than the design load; likely, many other Italian highway bridges with similar structural characteristics have a similar capacity.

Keywords Load test to failure · Structural health monitoring · Structural model · Model updating · Prestressed concrete bridge · Ultimate capacity

1 Introduction

The number of bridges approaching or exceeding their initial design life has increased dramatically over the last decade. The 2021 Report Card for America's Infrastructure [1] points out that 42% of all bridges across the United States are at least 50 years old; the average age of America's bridges is 44 years and 7.5% of them are considered structurally deficient. In Japan, around 25% of bridges (2 m long or longer) are at least 50 years old, and the number is expected to rise to 52% in 2029 [2, 3]. In Italy, we estimated that 50.4% of the highway bridges are at least 50 years old, and their average age is 48. Figure 1 shows the age of a sample of 1945 highway bridges, more than 65% of the Italian asset.

At the same time, bridges are withstanding an ever-increasing traffic volume, both in the number and the weight of vehicles. For instance, in the United States, the vehicle miles travelled reached more than 3.2 trillion in 2019, an increase of 18% from 2000 [1]. The US Standard [4], the European Standard [5], and the Italian Standard [6] have progressively increased the design traffic load over the years [7]; the current dimensional and mass limits imposed by national's Highway Codes [8–10] confirm such increment. All that increases the maximum load effects (e.g., shear force and bending moment) that ageing bridges may expect during their remaining life.

As civil infrastructures age, the investments required to maintain their performance and safety increase, along with the impact of bridges' failures on the economy, environment, and society [11–13]. Moreover, since a short-term substitution of all the structurally deficient bridges

✉ D. Tonelli
daniel.tonelli@unitn.it

[1] Department of Civil, Environmental and Mechanical Engineering, University of Trento, via Mesiano, 77, 38123 Trento, Italy

[2] Department of Civil and Environmental Engineering, University of Strathclyde, 75 Montrose St, Glasgow G1 1XJ, UK

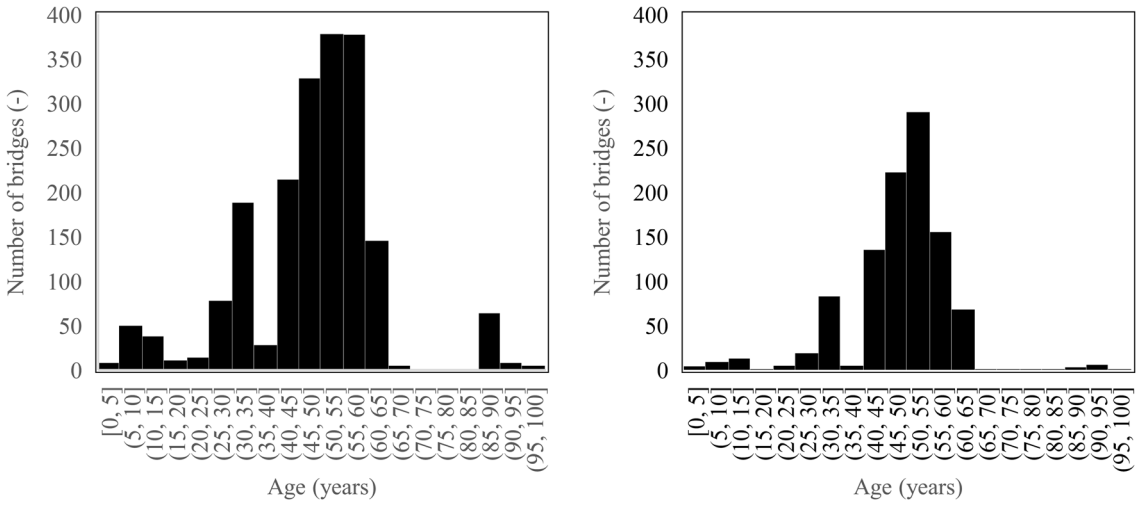

Fig. 1 **a** Age distribution among a sample of 1945 Italian highway bridges (more than 65% across the Nation); **b** age distribution among 1019 Italian PC highway bridges with simply supported spans (52% of the whole sample)

is economically and strategically impossible, the average age of bridges and the investments in maintenance will increase exponentially in the future. For instance, the 2020 USA's backlog of bridge repair needs is $125 billion, rising from $14.4 billion annually to $22.7 billion annually [1]. The American Society of Civil Engineers claims that at the current rate of investment, all the currently necessary repairs will take until 2071 and that the additional deterioration over the next 50 years will become overwhelming. In addition, since most goods and products are moved by trucks and trains, even short-term closure of strategic bridges can cause time-loss to drivers due to congestion and excessive damage to national economies [1].

As a result, it is crucial to frequently check bridges' deterioration, prioritise the maintenance within an infrastructure asset, and effectively assess bridges' performance and safety [14]. Non-destructive tests (NDTs) of material specimens and structural health monitoring (SHM) can measure and control the decay of the materials' properties and the variation in the structural behaviour of bridges in-service [15]. Numerical models of bridges can predict their response under operational and exceptional loads with low uncertainties [16]; however, such uncertainties increase as bridges age due to deterioration mechanisms. Moreover, real-life boundary conditions, connections between structural parts, and the soil–structure interaction may differ from what is defined in the numerical model and have an unexpected influence on the observed response. To cope with those problems, NDTs of material specimens and full-scale on-site load tests allow updating model parameters and obtaining predictions of bridges' responses as close as possible to the observed response.

Here, some questions arise. What behaviour can a structural model accurately predict? Are the model predictions in line with load test results? What is it possible to learn from a load test? How accurate are predictions after the model updating?

We presume that most careful readers are well aware that progressively refined levels of structural models and structural analysis exist in the scientific literature [17]: linear elastic, linear elastic with a limited redistribution, and plastic analysis with finite elements (FE), beam, frame or handbook methods; non-linear analysis reflecting flexural failures with FE; non-linear analysis reflecting flexural and shear-related failures with FE; and fully non-linear analysis reflecting flexural, shear-related, and anchorage failures with FE. Typically, predictions of the same structural response obtained from different structural models reveal significant variations. Predictions from refined models can be more accurate, but the analysis is more complex and may take a longer modelling and computational time. Moreover, assumptions on the geometry, boundary conditions, constitutive laws, and solution methods are necessary; thus, the outcomes are highly dependent on the modelling choices, which in turn depend on the analyst's experience [17].

Load tests allow calibrating prediction models and evaluating the performance of existing bridges [16, 18, 19]. Two load tests exist: diagnostic load tests and proof load tests. Diagnostic load tests involve loads lower than the design live load; they allow engineers to compare the observed response of the structure with the predictions of a structural model and update the model based on the results to make it verified in the field [16]. In contrast, proof load tests aim to verify whether a bridge can carry the prescribed factored live-loads

without distress [16]. Diagnostic load tests are suitable for in-service bridges, which should not experience damage during the test; therefore, only their linear elastic response is observable. However, the response of a structure to service loads is not necessarily representative of its response to higher loads due to non-linearities, stress redistribution, and other forms of interaction among elements. Collapse tests allow learning more about bridges' non-linear behaviour and ultimate capacity; however, the structure will be dismissed after the test.

By analysing several studies published in the scientific literature [20–23], we observed that, in general, (i) the comparison between models predictions and load tests results typically shows a good correlation for the linear elastic responses; (ii) the correlation decreases significantly after the first crack opens; and (iii) the ultimate capacity observed is lower than the model prediction due to shear failure, or higher due to a conservative estimate by the models. In particular, Bagge et al. [22] present a review of 30 concrete bridges of different types tested to failure between 1952 and 2014: almost a third of them resulted in unexpected types of failure, mainly shear instead of flexure; the differences between predicted and observed capacities often appeared to be a consequence of inaccurate representations of geometry, boundary conditions, and materials. Cai and Shahawy [23] point out that those differences might also be attributed to field factors (e.g., diaphragm action, parapet stiffening, concrete hardening, unintended composite action, and unintended bearing restraints), which usually increase the bridges' capacity, but are neglected during the design stages and in structural models. Also, harsh environmental conditions and the ageing of materials lead to a structural deterioration that affects the load-carrying capacities. For instance, corrosion degradation can produce concrete cracks that follow the trajectory of the post-tensioning tendons, reduce ductility, and halve the load capacity [24].

The correlation between predictions and observation also depends on the structural analysis performed. Pressley et al. [20] compare actual bending failure loads and ultimate loads predicted through progressively refined structural analysis. The standard 1D linear elastic analysis predicted the ultimate loads as 37–42% of the actual load, the 2D yield line predicted 81–96%, and the 3D non-linear FE analyses predicted 89–101%. They also claim that the analyses did not predict the general shear failure mode that accompanied the ultimate bending failure. Bagge et al. [17] confirm that a refined non-linear FE model can reproduce the actual structural behaviour, identifying the failure mechanism and predicting the actual load-carrying capacity with a difference of less than 3.8%.

Finally, many studies show that relatively small changes in the model parameters result in significant changes in the model predictions of the elastic response, load-carrying capacity, and failure mechanism [17, 23]. Sensitivity analyses point out that the most influential model parameters are the concrete compressive and tensile strength, concrete elastic modulus, level of residual stress in prestressing cables, and the boundary conditions at supports.

This paper gives an insight into the ultimate load-carrying capacities of existing prestressed concrete (PC) bridges and studies their response during a load test to failure. It compares the observed response of a PC bridge subjected to a controlled load test up to its failure, the Alveo Vecchio viaduct, with the responses predicted by four different structural models. An extensive SHM system measures the observed response. The structural models have different levels of refinement (two are analytical models, and two are finite-element models) and (different uncertainties in the input parameters (two have prior parameters, and two have parameters updated based on monitoring data). First, the paper discusses what engineers can observe and learn from a load test as the load progressively increases (e.g., stiffness, first-crack load, ultimate capacity). Then, it identifies the model parameters that influence the response prediction the most. Finally, it verifies whether a diagnostic load test carried on up until the design traffic load allows identifying the following states: (i) the structural response remains elastic during the entire load test; (ii) the bridge cracks during the load test; (iii) the bridge was already cracked before the load test.

We organised the manuscript as follows: Sect. 2 introduces the Alveo Vecchio viaduct; Sect. 3 illustrates the load test design, providing the details and the hypotheses of the four prediction models developed. Section 4 reports the load test execution: the agenda and the monitoring system results. Finally, Sect. 5 discusses the correlation between the models' predictions and the observed structure response. Conclusions are drawn in Sect. 6.

2 Case study

2.1 Alveo Vecchio viaduct

The Alveo Vecchio viaduct is part of the old track of the A16 Italian Highway. It was built in 1968 and decommissioned in 2005 after being hit by a landslide, which caused one pier's failure. It represents 52% of the Italian highway bridges in terms of structural type, age, and deterioration. The viaduct consists of two structurally independent decks, one for each carriageway, each made of three 32.5 m-long simply supported spans, with a slight slope of around 1.45%. Each span consists of four 2 m-high PC girders supporting a 20 cm-thick concrete slab. Five equidistant reinforced concrete cross-girders connect the longitudinal girders, one at the centre, two at the end, and the remaining two between

them. The bridge deck leans on fixed and free neoprene bridge bearings. Figure 2 shows a top view, a lateral view, and a cross-section of the viaduct. According to the design documentation [25], the prestressing was applied through 14 post-tensioned parabolic cables per girder, with an initial jacking tension of 1250 MPa. Each cable has an ultimate strength of 1700 MPa and a yielding strength of 1450 MPa. Figure 3 shows a transversal section of the girders with the prestressing cables. The wall piers are 3.30 m high and have deep foundations consisting of eight bored piles 23 m long with a diameter of 1.2 m. The abutments are founded on six bored piles with a diameter of 1.20 m. Additional information about the structure is found in [25].

The viaduct is 50 km far from the sea and surrounded by countryside. The winter temperature hardly goes below 5 °C; thus, the environment is not aggressive, and the viaduct is subject to limited use of de-icing salts. Visual inspections never reported signs of corrosion degradation, nor did we notice it in the steel specimens extracted for laboratory tests. In 2005, a landslide hits the C1sx and C1dx spans. It resulted in the collapse of span C1dx and the roto-translation of Pier 1. A preliminary visual inspection reported that the landslide did not affect spans C3sx and C3dx. Therefore, we chose span C3sx for the load test to failure reported in this paper.

2.2 MIMS Infrastructure Safety Test Field

Since June 2019, a research agreement has been active between the Italian Ministry of Sustainable Infrastructure

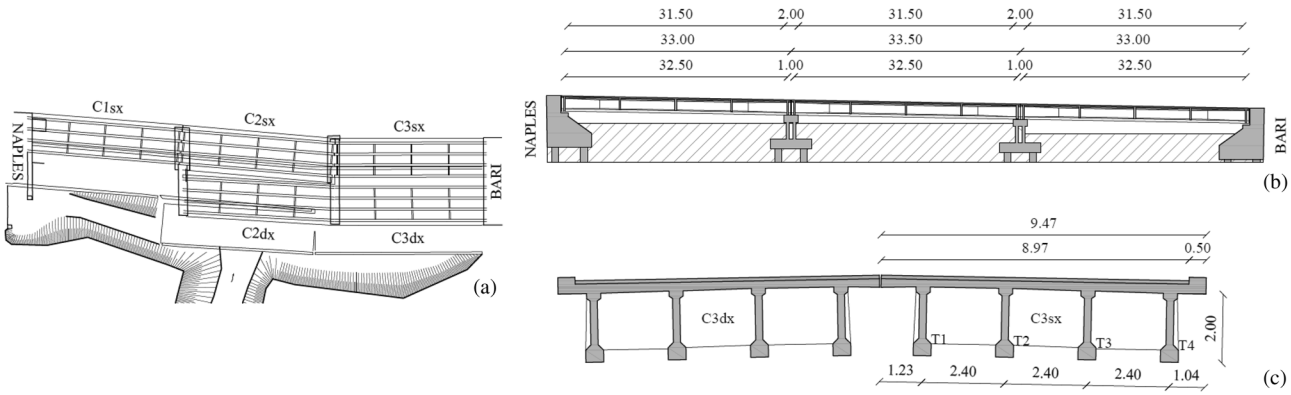

Fig. 2 **a** Top view; **b** lateral view; and **c** cross-section of the Alveo Vecchio viaduct (Italy)

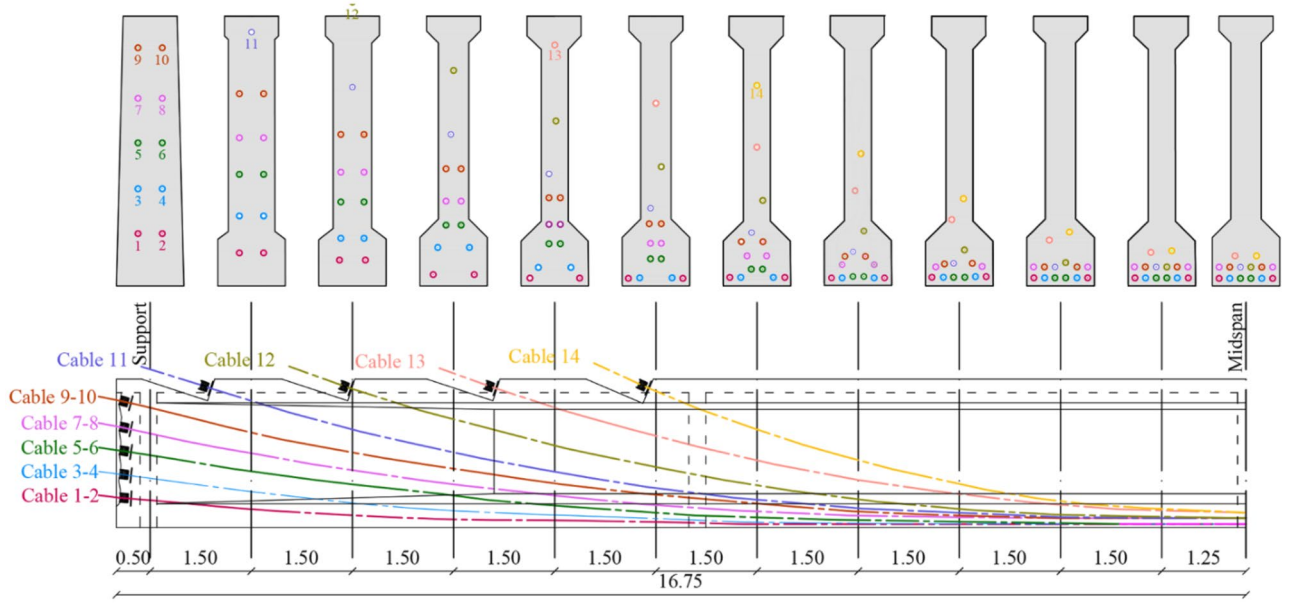

Fig. 3 Longitudinal and transversal section of girders with post-tensioned cables

and Mobility (MIMS), Autostrade per l'Italia SpA (the principal operator of Italian highways), and the University of Trento. This agreement concerns the management and monitoring of civil infrastructure, intending to develop survey protocols and monitoring systems to assess the safety and performance of existing highway bridges. It includes an extensive experimental activity that aims to validate the feasibility and effectiveness of methods for assessing the safety of existing bridges in actual conditions, including static and dynamic load tests and NDTs for the characterisation of materials.

The MIMS Infrastructure Safety Test Field was set up at the Alveo Vecchio viaduct: it is an open-air laboratory where the authors have the unique opportunity to test the performance of a bridge in actual conditions of degradation and constraint. The inaugural test was the load test to failure of an entire span, aiming to evaluate the ultimate capacity of an isostatic span built in 1968 and subject to routine maintenance. This article reports the results of this test.

The Alveo Vecchio test field was established under art. 14 of DL 28/09/2018, n.109, ("Genoa Decree") [26], which led to the release of an official document called "Italian guidelines for risk classification and management, safety assessment and monitoring of existing bridges" (LG20) [27]. Then, the DM 578 of 17/12/2020 [3] approved the introduction of these new guidelines as an experimental application related to the management and health monitoring of bridges and viaducts on a stock of infrastructures managed by several highways operators. The outcome of the experimentation described in this manuscript will provide an advanced and unified instrument, which, while overcoming the simple census of the existing bridges [28, 29], will allow the managing of risks as well as the security verification of the infrastructures through a general, multi-level, multi-criteria and multi-objective approach. According to LG20, the classification of bridges on a national scale consists of a simplified estimate of the risk factors associated with the artefacts, inspected, and recorded at various levels of verification. Thereby, the risk related to bridges is first evaluated approximatively through processing the results of visual inspections and successively incremented or decremented according to a simplified assessment of each structure's hazard, vulnerability, and exposure. As for post-tensioned PC bridges, however, visual inspections are not an effective tool to assess their conditions, not even approximate, since the cables are not visible. For such structures, it is necessary to proceed directly to more in-depth investigations. Currently, we are performing an increasingly complex campaign of extensive tests for a deepening level of knowledge of the structure and its components [30, 31]. It aims to define an adequate framework for investigating the state of decay of the existing PC bridges. The MIMS Test Field was established to identify those tests and the most effective investigations for assessing the condition of PC bridges.

3 Load test design

3.1 Load test protocol

The Alveo Vecchio viaduct was designed in 1966 by Eng. A. Passaro. He chose the design live-loads according to the Italian standards Circ. Min. LL.PP. 14/02/1962 n. 384 [32], and he calculated their effects on each girder through the Courbon method [33]. The design documentation [34] reports that the bending moment on the most stressed girders (externals) of span C3sx due to the design live-loads is 4259 kNm. We designed the load test protocol by choosing as the load unit the concentrated load that would have generated a bending moment equal to the design bending moment in the midspan cross-section of the most stressed girders (externals). As a result, the load unit was a 2400 kN concentrated load centred in the midspan applied over a footprint that extends for 7.35 m longitudinally.

Since 1962, vehicle's type, number, and mass have changed significantly. Therefore, we also calculated the highest bending moment on the most stressed girders of span C3sx considering the vehicles that nowadays can transit on the Italian highway network. The Italian Highway Code [10] defines the dimensional and mass limits; the current Italian standard DM 17/01/2018 [6] defines the width of the lines. We considered a train of 440 kN loads consisting of two 5-axle trucks and one 4-axle work vehicle with the characteristics shown in Fig. 4. We assumed that the vehicles are in a static configuration aligned at a distance of 1 m. The dynamic effect can be neglected for bridges with short spans like the Alveo Vecchio viaduct. We also assumed two load lanes of 3 m-width plus one of 2.75 m-width for the emergency lane. According to the Courbon method, the emergency lane implies a negative transverse partition coefficient; consequently, we consider the emergency lane unloaded. The bending moment resulting in the most stressed girders due to the real live-loads is 4853 kNm, which is 13.9% higher than the design bending moment.

We chose to apply the load equally distributed between the four girders to avoid introducing a hypothesis on the transverse flexural distribution. We designed the load unit as a matrix of 3×4 steel ballast weights with a size of $2.15 \times 1.60 \times 0.45$ m and a weight of 100 kN, each arranged in two layers. We planned to place the weights

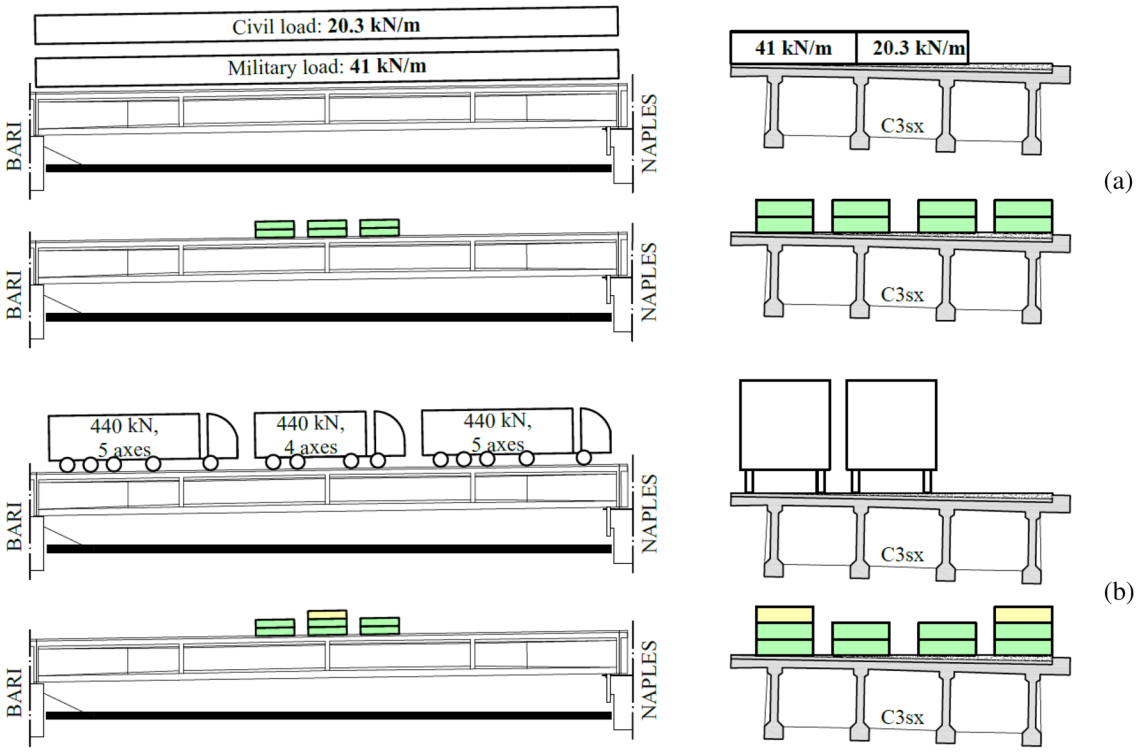

Fig. 4 **a** Live-loads configuration used to design the Alveo Vecchio viaduct; **b** most demanding live load configuration that can transit nowadays on Italian highways in compliance with dimensional and mass limits

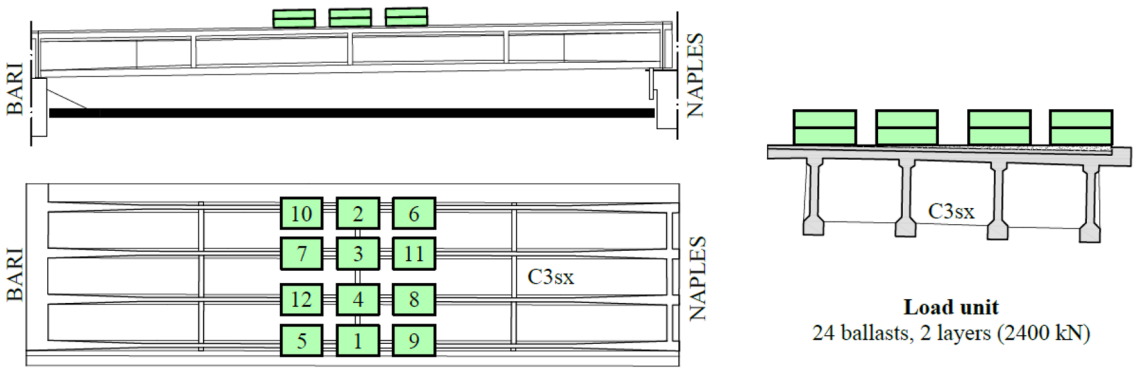

Fig. 5 Load unit configuration and sequence of weights application repeated for each layer

one by one on the bridge slab with a crane; Fig. 5 shows the load unit configuration and the sequence of applications to be repeated for each layer.

To collapse the viaduct, we planned to progressively increase the number of weights layers in multiples of the load units. As a result, we defined the following loading phases: P1—1200, P2—2400, P3—4800, P4—7200, and P5—9600 kN, each of them followed by the complete unloading of the bridge. Figure 6 shows the load test protocol for the load test of the span C3sx. We defined the stop criteria based on the midspan deflection. The load test had to stop if (i) the midspan deflection would have increased more than 50 mm after a new 100 kN weight application or (ii) the total midspan deflection would have exceeded 300 mm. To avoid the post-critical response of the structure, for safety reasons, and to save the equipment, we decided to perform the last loading phase, P5, in displacement control with four hydraulic jacks placed under the girders midspan.

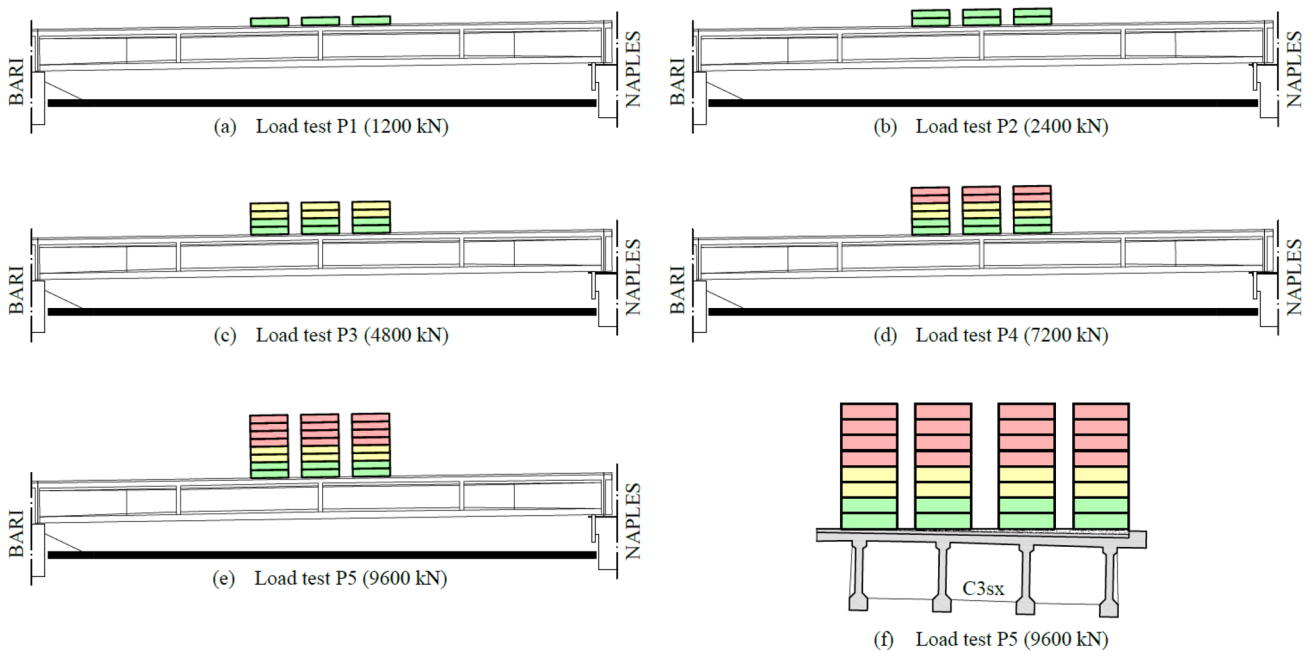

Fig. 6 Loading phases P1–P5 with a progressive number of steel ballasts. Colours: green is equivalent to the load unit; yellow is twice the load unit; red is 3 and 4 times the load unit (colour figure online)

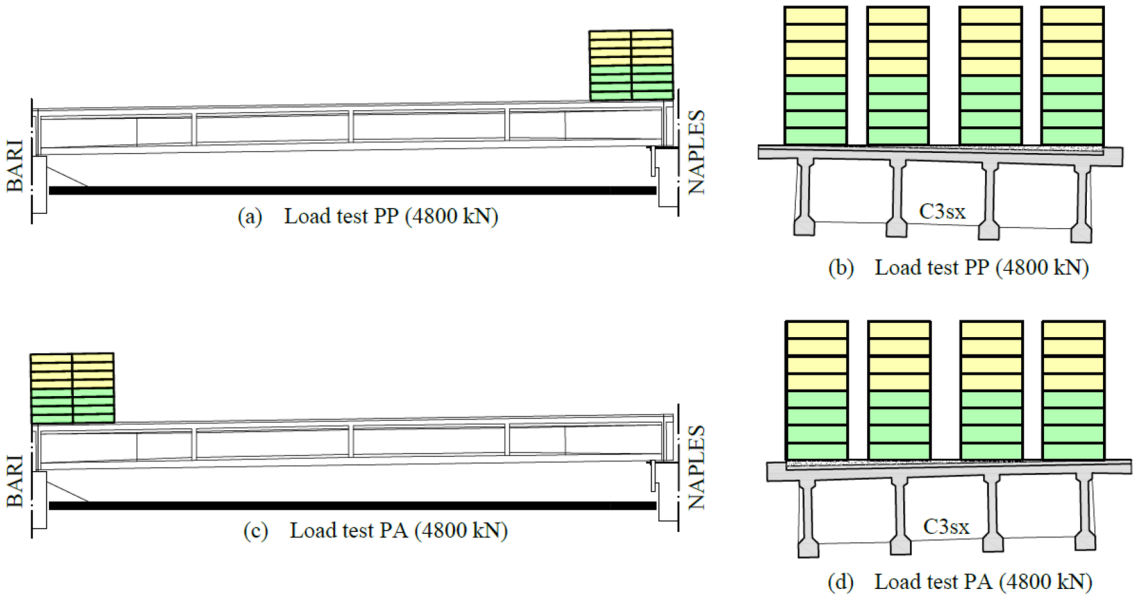

Fig. 7 Loading phases PP (weights on the pier) and PA (weights on the abutment) with 4800 kN each

To verify whether the span C3sx had been unaffected by the 2005 landslide, we performed two additional load tests before P1: one for the abutment and one for the pier. They confirmed the absence of abnormal settlement and rotation of foundations, which might have falsified the output of the load test. We tested the C3sx span's pier and abutment with 4800 kN each, as shown in Fig. 7.

3.2 Material properties

The design documentation did not report all the mechanical properties of the materials used to build the viaduct. For structural calculations, Eng. Passaro used concrete

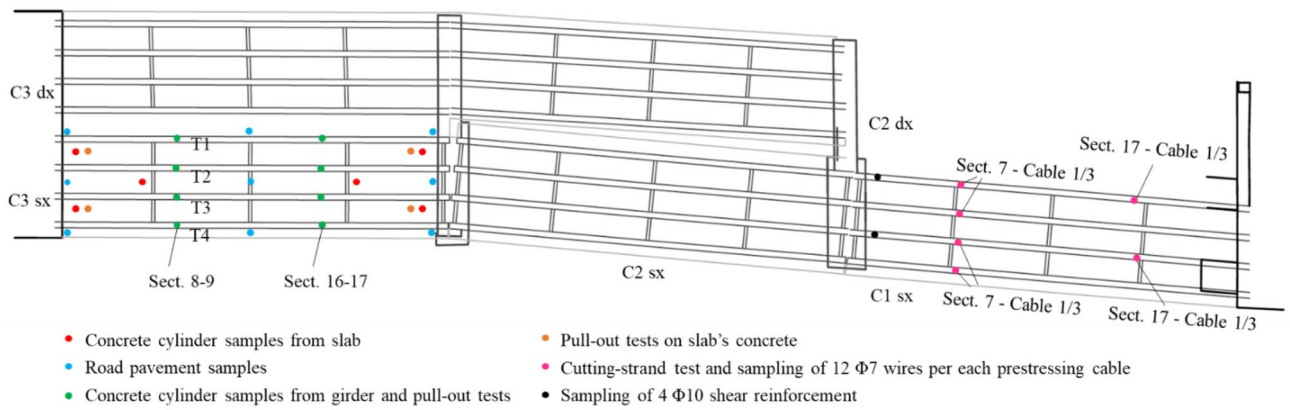

Fig. 8 Location of the extracted samples and NDTs along the viaduct

Table 1 Material properties of slab and girders estimated from NDTs

Location	Material	Property	Test	Unit	Mean value	Standard deviation	Coeff. of variation (%)
Slab	Concrete	Compressive cube strength	Pull-out	N/mm^2	38.37	3.33	8.68
Girder	Concrete	Compressive cube strength	Pull-out	N/mm^2	50.00	5.86	11.72
Girder	Concrete	Tensile strength	Brazilian	N/mm^2	2.2	0.34	15.5
Girder	Prestressing steel	Yield strength	Tensile	N/mm^2	1509.38	75.38	4.99
Girder	Prestressing steel	Ultimate tensile strength	Tensile	N/mm^2	1742.71	37.05	2.13
Girder	Prestressing steel	Strain at maximum load	Tensile	%	9.17	2.08	22.64
Girder	Prestressing steel	Residual stress	Strand-cut	N/mm^2	618.75	83.43	13.48
Girder	Reinforcement steel	Yield strength	Tensile	N/mm^2	398.97	79.03	19.81
Girder	Reinforcement steel	Ultimate tensile strength	Tensile	N/mm^2	614.23	48.63	7.92
Girder	Reinforcement steel	Strain at maximum load	Tensile	%	22.98	1.37	5.96

with a compressive strength of 40 MPa, prestressing steel with a failure strength of 1700 MPa, and reinforcement bars with an ultimate strength of 220 MPa.

We performed an extensive campaign of NDTs to characterise the properties of materials and provide the most accurate input parameters for the prediction models: dead loads g_1 and g_2 supported by the girders and the following properties:

- Concrete of girders and slab: compressive strength, tensile strength, and elastic modulus.
- Prestressing steel: yield strength, ultimate tensile strength, strain at maximum load, and residual stress.
- Reinforcement steel: yield strength, ultimate tensile strength.

For this purpose, we performed the following tests (divided based on the material investigated):

- Concrete from girders and slab: 18 compression tests on cylindric samples, 18 pull-out tests, 5 indirect tensile tests (Brazilian test), 27 density measurements, and 9 carbonation tests.
- Reinforcement steel: 12 tensile stress tests.
- Prestressing steel: eight strand-cutting tests of single wires for residual prestress, 12 × 6 tensile stress tests according to EN ISO 15630-1:2010 [35] yield stress, ultimate tensile stress, and strain at maximum load (12 wires per 6 cables).
- Road pavement: four density and thickness measurements.

Figure 8 shows the location of the extracted samples along the viaduct. We extracted most of the samples from the C3sx span's elements to accurately estimate its material properties before the load test; in contrast, we sampled the shear reinforcement steel and performed strand-cutting tests on the C1sx span to avoid reducing the C3sx span's

Table 2 Effects of dead loads g_1 and g_2 on girders T1, T2, T3, T4

Girder	T1	T2 and T3	T4
M_{g1+g2} [kNm]	6231	5811	5588
V_{g1+g2} [kN]	739	687	659

performance. Table 1 shows the properties of the materials obtained from direct and indirect tests with their mean value, standard deviation, and coefficient of variation. Table 2 reports the effects of dead loads on the girders based on different portions of the slab supported by them.

3.3 Prediction models

3.3.1 Hypotheses on the properties of materials

We assumed the distributions of NDTs results as Gaussian. Based on those distributions, we defined three hypotheses on the mechanical properties of materials, summarised in Table 3, as inputs of the prediction models:

- Hp. A: 5% fractal of the distribution of NDTs results, with some variations.
- Hp. B: 50% fractal (average value) of the distribution of NDTs results, with some variations.
- Hp. C: 95% fractal of the distribution of NDTs results, with some variations.

3.3.2 Structural models

First, we developed an analytical model called ANA1 for designing the load test. We predicted the structural capacity in terms of bending moment and shear force. We compared them with the structural demand resulting from the increasing number of steel ballasts on the bridge. Model ANA1 is based on the design documentation and NDTs on material specimens only, without any evidence of the actual response during the load test.

Then, we updated the analytical model ANA1 into the analytical model ANA2 during the load test, once the first cracks had opened, by changing the residual stress to make the first crack loads (one for each girder) predicted by the numerical model equal to the observed ones. Therefore, model ANA2 is based on the design documentation, NDTs, and a diagnostic load test on the bridge until the first crack opening. Results from model ANA2 defined the load-test stop criteria.

After the conclusion of the load test, we developed a finite-element model, FEM1, with the same hypotheses as model ANA2, aiming to interpret the test results better.

Table 3 Three hypotheses on the mechanical properties of materials based on the results from the non-destructive tests

Location	Material	Property	Unit	Hypothesis A		Hypothesis B		Hypothesis C		Notes
				Fractal	Value	Fractal	Value	Fractal	Value	
Slab	Concrete	Compressive cylinder strength	N/mm^2	5%	27.3	50%	31.9	95%	36.4	
Slab	Concrete	Elastic modulus	N/mm^2	5%	29,323	50%	31,942	95%	34,561	[a]
Girder	Concrete	Compressive cylinder strength	N/mm^2	5%	33.5	50%	41.5	95%	49.5	
Girder	Concrete	Tensile strength	N/mm^2	–	0	5%	2.18	5%	2.45	[b, c]
Girder	Concrete	Elastic modulus	N/mm^2	5%	30,774	5%	33,523	95%	36,272	[a]
Girder	Prestressing steel	Yield stress	N/mm^2	5%	1385	50%	1509	95%	1633	
Girder	Prestressing steel	Ultimate tensile strength	N/mm^2	1.49‰	1485	1.49‰	1618	1.49‰	1751	[d]
Girder	Prestressing steel	Strain at maximum load	%	Design value	3.5	1.49‰	4.43	1.49‰	6.06	[d, e]
Girder	Prestressing steel	Residual stress	N/mm^2	5%	482	50%	619	Design value	1000	
Girder	Reinforcement steel	Yield stress	N/mm	5%	269	50%	399	95%	529	
Girder	Reinforcement steel	Ultimate tensile strength	N/mm^2	5%	534	50%	614	95%	694	

[a] $E_{cm} = 22\ (f_{cm}/10)^{0.3}$ from EN 1992-1-1:2004, Table 3.1 [36]: Hp. A: $E_{ck;0.05} = E_{cm}(1 - 1.645\ CV)$ and $CV = 5\%$, Hp. C: $E_{ck;0.95} = E_{cm}(1 + 1.645\ CV)$ and $CV = 5\%$

[b] Hp. A: the first crack has already opened; therefore, we assume a zero tensile strength of the concrete, $f_{ct} = 0$ MPa

[c] $f_{ctk;0.05} = 0.7\ f_{ctm}$, where $f_{ctm} = 0.3\ f_{ck}^{2/3}$ from EN 1992-1-1:2004, Table 3.1 [36], and: Hp. B: $f_{ck} = f_{cm} - 8$; f_{cm} from pull-out tests, Hp. C: $f_{ck} = f_{cm} - 1.645\sigma$; f_{cm} and σ from pull-out tests

[d] 1.49‰ of the distribution f_i/f_{ym}, with f_{ym} the yield stress of the same hypothesis; 1.49×10^{-3} is (number of prestressing wires tested)$^{-1}$, because we consider that the structural collapse occurs when the first prestressing wire fails

[e] Hp. C: average value of the more likely values; we considered a few values as outliers

Finally, we updated model FEM1 into model FEM2, changing the most influential parameters according to a sensitivity analysis (e.g., the elastic modulus of the concrete and the residual stress of prestressing cables) aiming to make the model predictions as similar as possible to what was observed by the monitoring system.

In this section, we illustrate only the hypotheses of the four prediction models; we will show their results and the model updating procedure in Sect. 5.

3.3.2.1 Model ANA1 Models ANA1 and ANA2 consider the following parameters as deterministic:

- Ultimate strain of concrete $\varepsilon_{cu} = 0.35\%$.
- Elastic modulus of the prestress steel: $E_s = 200$ GPa;
- Effects of dead loads g_1 and g_2 resulting from the NDTs (see Sect. 3.2).

Moreover, we implemented the following stress–strain relation curves of materials:

- Parabola–rectangle diagram for concrete under compression from EN 1992-1-1:2004 [36];
- Bilinear diagram for harmonic and reinforcing steel: linear elastic up to the yield strain, with a further increase between the yield and the ultimate strain.

We calculated the shear resistance of the girders over the pier and abutment with equations for the design shear resistance of the member without shear reinforcement from EN 1992-1-1:2004 [36], and the ultimate moment resistance of the prestressed concrete midspan cross-section of each girder with equations from EN 1992-1-1:2004 [36]. Regarding the ultimate moment resistance, we assumed different inertial properties of the girders: T2 and T3 have the same geometry, T1 supports a wider slab (0.270 vs. 0.240 m), and T4 supports a shorter slab with an additional curb, which significantly increases the stiffness. Table 4 shows the moment and shear resistance of each girder predicted by model ANA1.

3.3.2.2 Model ANA2 We updated model ANA1 into model ANA2 by changing the residual stress $\sigma_{p,\infty}$ in the material hypotheses, and we removed hypothesis A since it seemed excessively precautionary. Table 5 shows the updated value of residual stress.

Table 5 The updated value of residual stress $\sigma_{p,\infty}$ for each girder and hypotheses B and C implemented in ANA2

Hypothesis	Residual stress $\sigma_{p,\infty}$ [MPa]			
	T1	T2	T3	T4
B	1030	975	980	1005
C	955	980	1020	950

3.3.2.3 Model FEM1 We designed the finite-element model FEM1 with the open-source software OpenSees developed by PEER (Pacific Earthquake Engineering Research) [37]. We considered only the material hypothesis C as defined for model ANA2, and we modelled each girder with frame elements with fibre section to permit the spread of plasticity and better simulate the girders' geometry and the position of the prestressing cables along the girder. Each fibre had the following non-linear stress–strain relations already implemented in OpenSees [38]:

- "Concrete 04—Popovics Concrete Material" for the concrete.
- "Steel04 Material" for the harmonic steel.
- "Steel02 Material—Giuffré-Menegotto-Pinto Model with Isotropic Strain Hardening" for the steel reinforcement.

We discretised each girder in 24 frame elements. We modelled the cross-girders as rectangular connecting elements, adding a portion of the collaborating slab to simulate its orthogonal stiffening effect. Figure 9 shows the number and length of each element and a girder modelled with a frame element with a fibre section. We modelled the span as simply supported by adding one pinned support over the abutment and one roller support over the pier for each girder.

3.3.2.4 Model FEM2 We updated model FEM1 into model FEM2 by changing the residual stress of prestressing cables $\sigma_{p,\infty}$ and the elastic modulus of the concrete E_c in

Table 4 Ultimate moment and shear resistance for each girder predicted by the structural model ANA1

Hypothesis	T1		T2		T3		T4	
	M_R [kNm]	V_R [Nm]	M_R [kNm]	V_R [Nm]	M_R [kNm]	V_R [Nm]	M_R [kNm]	V_R [Nm]
A	19,748	1359	19,521	1359	19,521	1359	19,990	1359
B	21,777	2984	21,535	2984	21,535	2984	21,605	2984
C	23,347	5240	23,155	5240	23,155	5240	23,260	5250

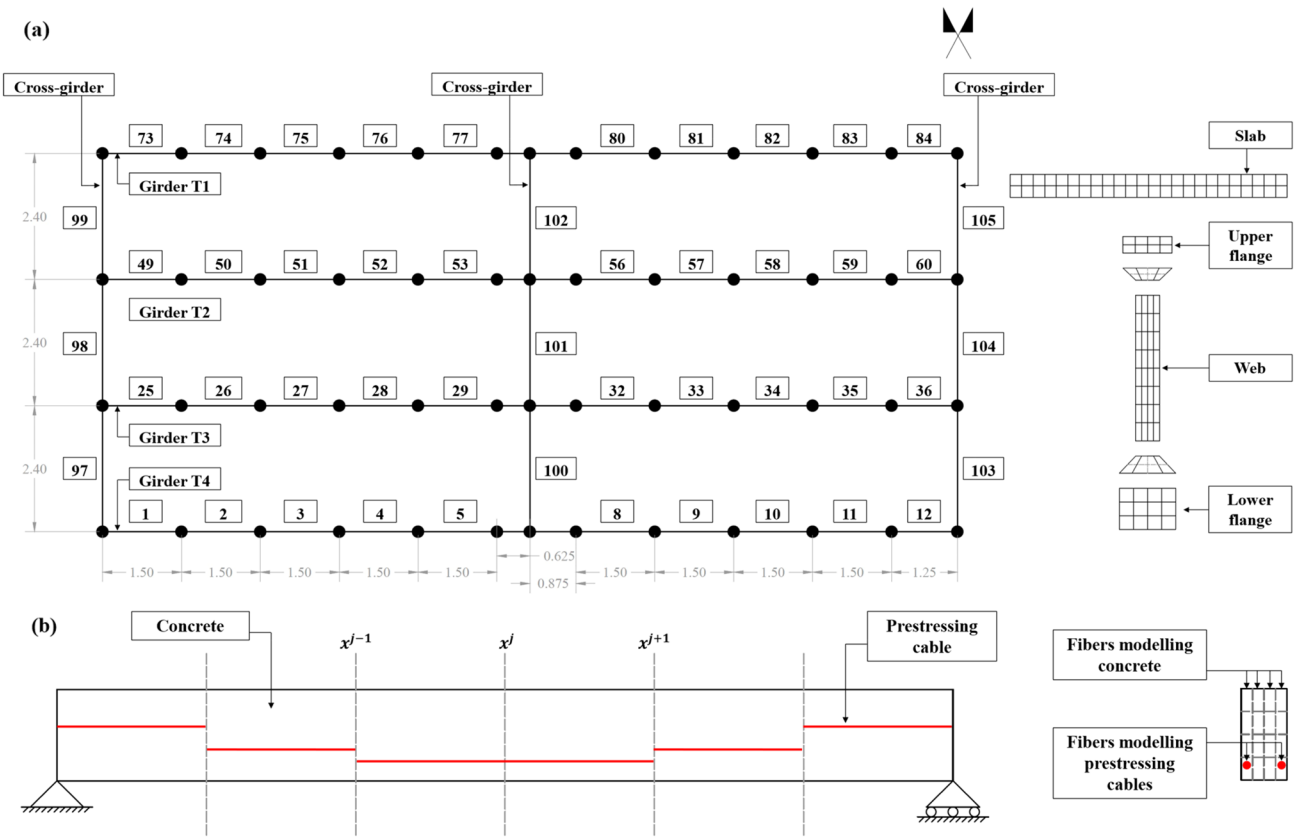

Fig. 9 **a** Discretisation of (**a**) the bridge span and girders and **b** the prestressing cables in frame finite elements with fibre section

Table 6 The updated value of the residual stress $\sigma_{p,\infty}$ and the elastic modulus E_c of the concrete for each girder implemented in FEM2

Parameter	T1	T2	T3	T4
Residual stress $\sigma_{p,\infty}$ [MPa]	696	794	820	950
Elastic modulus E_c	39,899	39,899	39,899	39,899

each girder to better simulate the response of the viaduct observed by the monitoring system during the load test. We identified such values with a sensitivity analysis described in Sect. 5.2.4; Table 6 reports them.

Table 7 Load test calendar with date and time of each loading and unloading phase

Phase	Description	Data	Start loading	End loading	Start unloading	End unloading
P0	Environmental live-loads	26/06–01/07/2019	–	–	–	–
PP	Pier 4800 kN	01/07/2019	16:15	21:27	10:04[a]	18:06[a]
PA	Abutment 4800 kN	02/07/2019	10:04	18:06	6:40[a]	12:30[a]
P1	Midspan 1200 kNt	04/07/2019	7:22	8:19	9:55	10:30
P2	Midspan 2400 kN	05/07/2019	10:30	12:27	13:20	16:00
P3	Midspan 4800 kN	08/07/2019	12:00	18:45	7:30[a]	14:49[a]
P4	Midspan 7200 kN—Part 1	10/07/2019	6:30	13:57 (4800 kN)	–	–
	Midspan 7200 kN—Part 2	11/07/2019	6:30 (4800 kN)	13:37 (7200 kN)	15:48 (720 t)	18:09 (480 t)
	Midspan 7200 kN—Part 3	12/07/2019	–	–	8:47 (480 t)	12:40
P5	Midspan 9600 kN—Part 1	21/07/2019	13:15	18:00 (4800 kN)	–	–
	Midspan 9600 kN—Part 2	22/07/2019	6:45 (4800 kN)	15:23 (9300 kN)	16:45 (9300 kN)	21:20 (6000 kN)
	Midspan 9600 kN—Part 3	23/07/2019	–	–	08:58 (6000 kN)	13:10

[a]Of the following day

Fig. 10 Pictures of the Alveo Vecchio viaduct during the loading phases: **a** PP–4800 kN; **b** PA–4800 kN; **c** P1–1200 kN, **d** P2–2400 kN, **e** P3–4800 kN, **f** P4–7200 kN, and **g** P5–9600 kN

4 Load test execution

4.1 Calendar

From 26 to 30 June 2019, a monitoring system (see Sect. 4.2) measured the bridge's response to environmental live-loads, measurements necessary for the temperature compensation of data acquired during the load test (see Sect. 4.3.2). The load test started on 1 July 2019 with the loading of the pier (phase PP), which was unloaded the day after by moving the steel ballasts progressively from the pier to the abutment (phase PA). The flexural load test of the span started on 4 July 2019 and continued until 23 July 2019, when it ended at 9300 kN once the stop criterion occurred. Table 7 reports the calendar: some loading and unloading phases lasted more than 1 day; weights were placed with an almost constant frequency of one ballast every 5 min. Figure 10 shows pictures of the bridge loaded at the end of all the loading phases.

Table 8 Objectives, key parameters, and measured quantities defined to design the structural health monitoring system

Structural behaviour during the load test			Real-time structural response and stop-criteria verification		
Objective	Key parameter	Measurement	Objective	Key parameter	Measurement
Structural distortion	Girder's deflection	Girder displacement	First-crack opening	Strain at the bottom of the midspan girders	Strain at the bottom of girders
	Pier and abutment settlement and inclination	Pier and abutment displacement and rotation			
	Bearings' crushing				
Damage identification	Crack's initiation and propagation on girders	Strain at the bottom of girders	Non-linear behaviour	Midspan deflection	Girder displacement
	Structural stiffness variation	Acoustic emission			
		Experimental modal analysis			
Thermal effects	Distortions due to temperature gradients	Temperature	Failure	Midspan deflection	Girder displacement

4.2 Structural health monitoring system

We designed the SHM system based on the Italian Guidelines for structural health monitoring, UNI/TR 11634:2016 [39, 40]. First, we identified the key parameters representing: the bridge response, the damage propagation during the load test, and the stop criteria. Then, we defined the type and position of measurements required to calculate the key parameters and chose the sensors' technology.

4.2.1 Key parameters

We defined two sets of key parameters: (i) key parameters to represent the structural behaviour during the load test; (ii) key parameters to identify in real time the structural response and damage condition and verify the stop criteria. Table 8 summarises the objectives, the key parameters, and the quantities we chose to measure to monitor the response of the bridge.

Table 9 Measured quantity, location, performance, number, and other characteristics of sensors. (displ. = displacement)

Quantity	Location	Unit	Sensor	Model	Manufacturer	Full-scale (FS)/range	Accuracy/resolution	No.
Girders' deflection	Bearings, *L*/4, *L*/2, 3/4*L*	mm	Wire displ. transducer	PT1DC-2 PT1DC-5	Celesco	50 mm 100 mm	0.28% FS	202
Girders' deflection	*L*/4, *L*/2, 3/4*L*	mm	Wire displ. transducer	PT1DC-20	Celesco	500 mm	0.18% FS	12
Displacement	All bridge	mm	Digital level and optical prism	LS10 0.3 mm	Leica	Min: 1.8 m Max: 110 m	Height: 0.3 mm Dist: 15 mm	18
Settlement	Abutment, pier	mm	Rectilinear displ. transducer	PZ12-50	Gefran	50 mm	–	8
Inclination	Abutment, pier, girders	°	Biaxial el-tiltmeter	–	Earth System	±5°	0.001°	12
Crack opening	Midspan T1, T4	mm	Rectilinear displ, transducer	PZ12-A-25 PZ12-100	Gefran	25 mm 100 mm	±0.01% FS	184
Temperature	Distributed	°C	Resistance thermometer	PT100	Earth System	− 50/+250 °C	0.2 °C	16
Deformation	Top slab	με	Rectilinear displ. transducer	PZ12-A-25	Gefran	25 mm	–	3
Acceleration	Girders T1, T4	mg	Accelerometer	393B12	PCB	±0.5 g pk 0.15–1000 Hz	0.000008 g rms	15
Acoustic emission	Midspan T2, T3	mg	Accelerometer	42A18	Endevco	±10 g 50–10 kHz	–	4

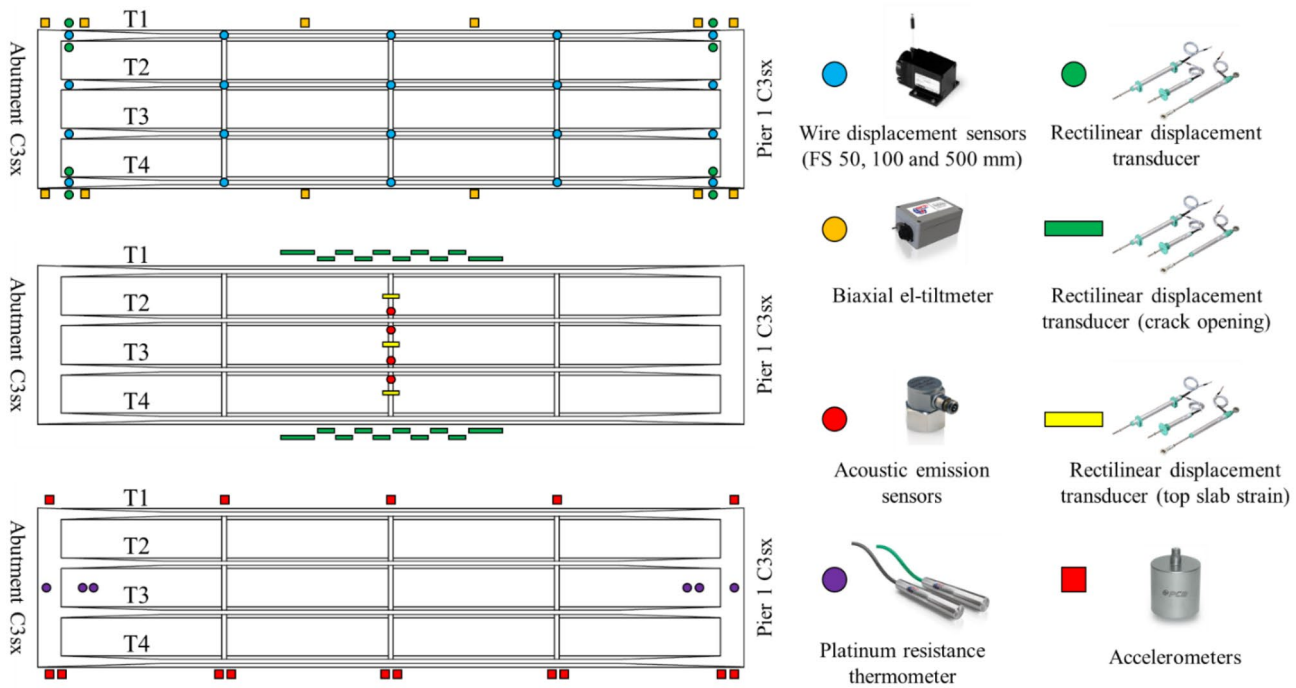

Fig. 11 Layout of the structural health monitoring system installed on the Alveo Vecchio viaduct during the load test

4.2.2 System technology

Based on key parameters and quantities to be measured, we identified the type and required performance of the sensors. Table 9 provides technical details of the monitoring system designed, which consists of 119 sensors divided into eight types: wire displacement sensors, deformation sensors, crack-opening sensors, electronic level, temperature sensors, inclinometers, accelerometers, and acoustic emission sensors. We also monitored air temperature, air humidity, and wind speed.

4.2.3 System layout

Figure 11 shows the monitoring system layout: (a) wire displacement sensors for measuring the deflection of girders, rectilinear displacement transducers for the crushing of bearings and the settlement of pier and abutment, and biaxial tiltmeters for the inclination of the pier, abutment, and girders; (b) rectilinear displacement transducers for cracks opening and top slab deformation, and acoustic emission sensors; and (c) platinum resistance

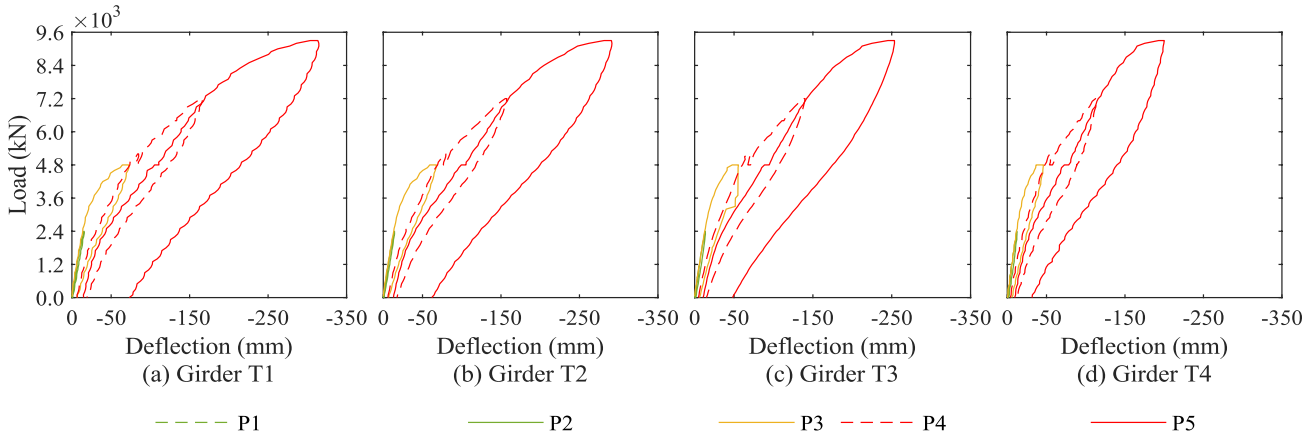

Fig. 12 Deflection of the girders midspan plotted against the load measured during the loading phases P1–P5

thermometers for temperature and accelerometers for dynamic monitoring.

4.3 Observed response

During the load test, the monitoring system acquired a large amount of data. We present and discuss only the most significant ones for the representation of the bridge's response and make a comparison with the prediction of models.

4.3.1 Direct measurements

4.3.1.1 Deflection of girders The deflection of girders is significant, because (i) we defined the stop criteria in terms of deflection measurements, and (ii) we aimed to compare the deflection measured during the test with those predicted by the structural models. Figure 12 shows the deflection observed at the midspan of the girders against the load placed during the loading phases P1–P5. It is possible to recognise stage I—elastic, between 0 and 3600 kN; stage II—cracks initiation and propagation, between 3600 and 8700 kN; and stage III—after the yielding of post-tensioned cables of all girders, over 8700 kN. The stop criterion, a total deflection of a girder higher than 300 mm, was reached during the loading phase P5 by the girder T1 for a load of 9300 kN; thus, we stopped the load test.

Figure 13 shows the longitudinal deformed shape of each girder at the end of each loading phase. The deflection was measured close to the bearings, at $L/4$, $L/2$, and $3L/4$, where L is the length of the span. The girder T1 experienced the highest deflection; the other girders' deflection decreased progressively toward T4. As a result, the bridge deck experienced a visible torsion. Possible reasons are the different geometry of the girder T4 due to the curb, the loads' redistribution due to the cross-girders, and a different crack-propagation and stiffness variation among the girders.

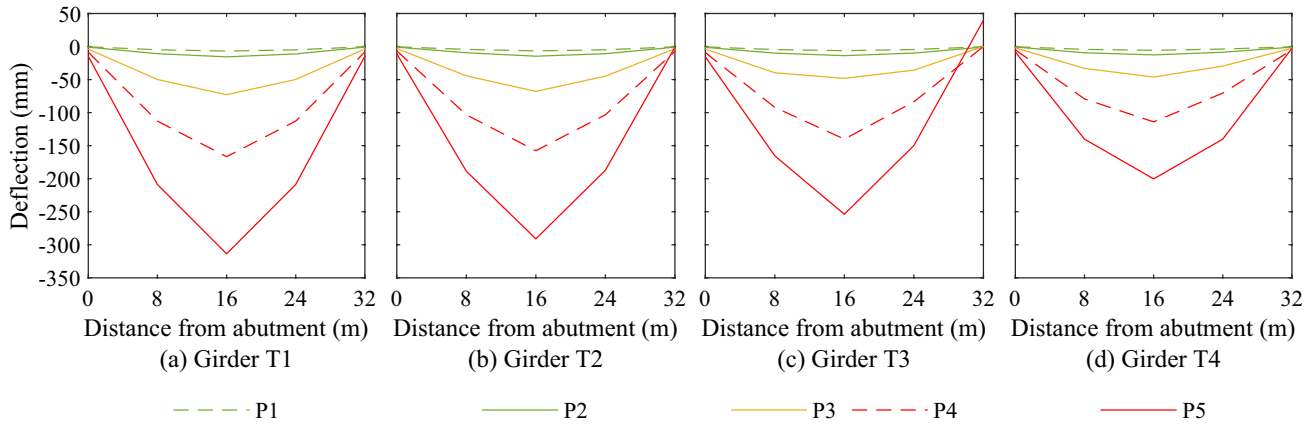

Fig. 13 Longitudinal deformed shape of girders: **a** T1, **b** T2, **c** T3, and **d** T4 at the end of each loading phase

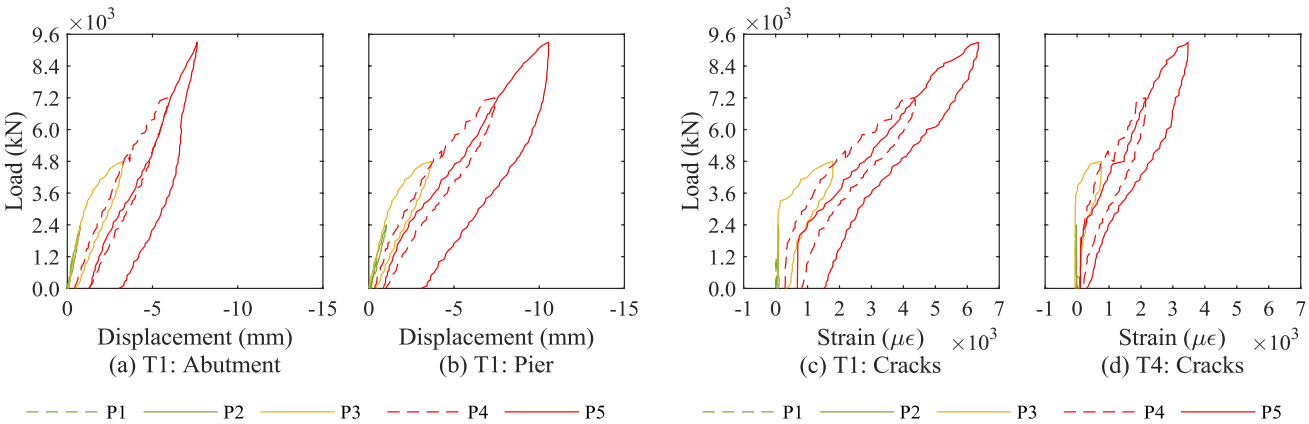

Fig. 14 Vertical deformation of elastomeric bearings of girder T1 over **a** the abutment and **b** the pier; longitudinal strain measured at the bottom of the midspan of girders: **c** T1 and **d** T4 during the load test

4.3.1.2 Crushing of bearings The bearings were elastomeric pads. They experienced a vertical elastic deformation up to 1.030 mm during loading P1 and P2. At the end of the load test (P5), they accumulated a plastic deformation of 3.067 mm. As a result, the deflection of girders reported in Figs. 12 and 13 is not significantly affected by the bearings' vertical deformation. Figure 14a, b shows the vertical deformation of T1 bearings over the abutment and the pier.

4.3.1.3 Settlement of foundations During the load test, we did not record relevant settlement of the abutment and pier foundations of span C3sx, which confirmed that the 2005 landslide did not compromise their capacity. We measured settlements of around 0.1 mm during the load phases P1 and P2, 0.4 mm during P3 and P4, and 0.6 mm during P5. As a result, the deflection of girders reported in Fig. 12 is not affected by the settlement of foundations.

4.3.1.4 Rotation of pier and abutment We did not record relevant rotation of the abutment and pier during the load test. The measured inclination was always lower than 0.1°. This result confirms that the abutment and pier foundations did not lose capacity due to the 2005 landslide. As a result, the deflection of girders reported in Fig. 12 is not affected by abutment or pier inclination.

4.3.1.5 Crack opening Figure 14c, d shows the longitudinal strain measured by crack-opening sensors at the bottom of the middle cross-section of girders T1 and T4, respectively. Girder T1 experienced a significant change in the strain at 3300 kN during the load phase P3 (solid amber line in Fig. 14a), which marks the opening of the first crack and a change of the girder's structural response from state I (elastic) to state II (cracked). On the other hand, girder T4 experienced the opening of the first crack at 4000 kN (solid amber line in Fig. 14b), which confirms the difference in the girders' stiffness starting from P3 and explains the highest deflection of T1 than T4. Figure 15 shows the crack pattern on girder T4 at the end of the load test. The amber and red triangles represent the propagation of cracks from phase P3 to phase P5: amber triangles mark the end of cracks after phase P3—4800 kN, single red triangles mark the end of cracks after phase P4—7200 kN, and double red triangles mark the end of cracks after P5—9300 kN. Girders T2, T3, and T4 have a similar crack pattern.

4.3.1.6 Acoustic emission We analysed the AE signals recorded during the load test and extracted the following parameters: amplitude, signal strength (MARSE), and peak frequency. A comprehensive report of the results and an in-depth discussion are in [30]. Our analysis focuses on AE results from the girder T2; they show the opening of the first crack at 4300 kN. That is in contrast with the measurements of the crack-opening sensors. Crack opening sensors on girder T1 point out that the first crack opened at 3300 kN (Fig. 14a). This difference can be explained by the difference in the girders monitored by the two technologies: girder T1 by crack-opening sensors and girder T2 by AE sensors. The girder T1 experienced the highest deflection and deformation; therefore, it is reasonable to assume that cracks have opened first on the girder T1 and then on the others.

4.3.2 Temperature compensation of measurements

It is commonly recognised that the response of a civil structure is significantly influenced by temperature variations [41, 42]. For this reason, we performed a temperature compensation [14] of the measurements acquired by the monitoring system to remove temperature effects from the structure's response and analyse only the response to the load progressively applied.

Based on the measurements of the bridge response to environmental live-loads recorded during phase P0 (mainly the variation of temperature), we found a correlation between the temperature in concrete and the sensors' measurements. Those are the steps that we followed: (1) we measured the temperature with 12 PT100 sensors in different portions of the bridge; (2) we limited the number of temperatures to three principal components using the Principal Component Analysis [43] to reduce the complexity of the problem; (3) we used a linear interpretation model to fit

Fig. 15 Visible cracks on the middle portion of girder T4 opened during the loading phases P3 (amber triangles), P4 (red single triangles), and P5 (red double triangles) (colour figure online)

Table 10 Non-compensated (NC) and temperature compensated (TC) deflections, concrete strain, and crushing of bearings measured on the girder T1 during the loading phases P1, P2, and P3

Measurement	Location	Unit	P1—1200 kN		P2—2400 kN		P3—4800 kN	
			NC	TC	NC	TC	NC	TC
Deflection	Midspan	mm	− 6.287	− 6.287	− 15.60	− 15.91	− 72.87	− 73.29
Concrete strain	Bottom of the midspan	με	48.40	53.60	178.8	171.2	1445	1436
Crushing of bearings	Abutment	mm	− 0.2998	− 0.2790	− 0.7692	− 0.7869	− 3.291	− 3.329
Crushing of bearings	Pier	mm	− 0.4471	− 0.4402	− 1.030	− 1.024	− 3.667	− 3.687

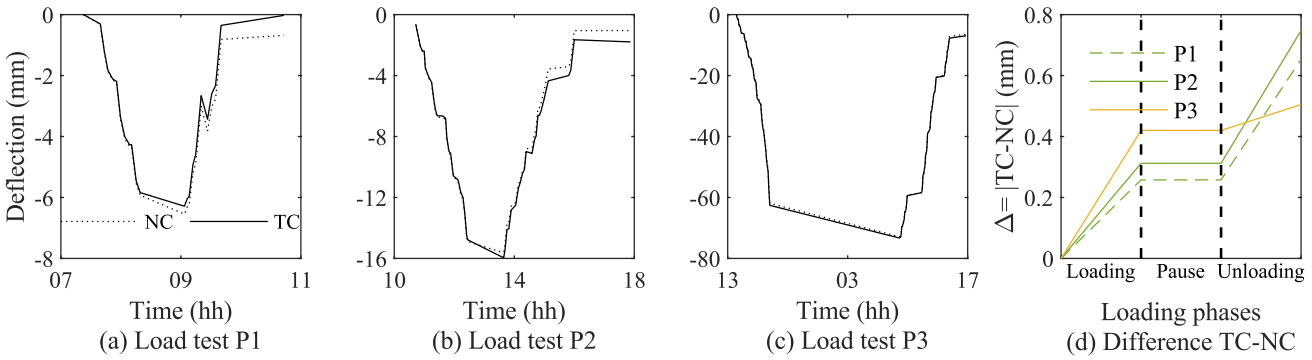

Fig. 16 Non-compensated (NC) and temperature compensated (TC) deflections measured at the midspan of the girder T1 during the loading phase: **a** P1, **b** P2, and **c** P3. **d** Difference between TC and NC deflections during loading phases P1, P2, P3

Table 11 Errors without operating the temperature compensation: e is the absolute value of the error and e/m is the relative value of the error, obtained by dividing the absolute value e with the non-temperature-compensated measurement m

Measurement	Location	Unit	P1—1200 kN		P2—2400 kN		P3—4800 kN	
			e [unit]	e/m [%]	e [unit]	e/m [%]	e [unit]	e/m [%]
Deflection	Midspan	mm	0.2577	4.100	0.3122	1.962	0.4199	0.5729
Concrete strain	Bottom of the midspan	με	5.541	11.49	7.601	4.247	8.774	0.6071
Crushing of bearings	Abutment	mm	2.078×10^{-2}	7.448	1.768×10^{-2}	2.247	3.785×10^{-2}	1.137
Crushing of bearings	Pier	mm	6.920×10^{-3}	1.5719	5.996×10^{-3}	0.5855	1.968×10^{-2}	0.5338

the measurements, and we estimated the model parameters through a least-squares regression using the software MATLAB; (4) eventually, we calculated the thermal-compensated values by subtracting the terms related to the temperature measurements Δ. The linear interpretation model used to fit the monitoring data is

$$\hat{\varepsilon} = \varepsilon_0 + mt + \alpha_1 T_1 + \alpha_2 T_2 + \alpha_3 T_3 = \varepsilon_0 + mt + \Delta, \quad (1)$$

where $\hat{\varepsilon}$ is the total strain, ε_0 is an offset parameter representing the ideal strain at time t_0 and temperature T_0, m is the variation trend over time, t is the instant of time considered, α is the apparent thermal expansion coefficient (i.e., it takes into account the changing of the strain as a function of the temperature), and T_i are the principal components of the temperature.

Table 10 and Fig. 16 show the results of the temperature compensation of the measured response of the girder T1.

The temperature compensation proved necessary to provide more detailed information on the structure, especially for low load levels. Table 11 shows the error we would have committed without operating the temperature compensation. The temperature compensation gives symmetry to the response measured during loading and unloading, especially for tests with low loads. The symmetry is a key parameter to ensure that the bridge did not experience permanent damage during the test.

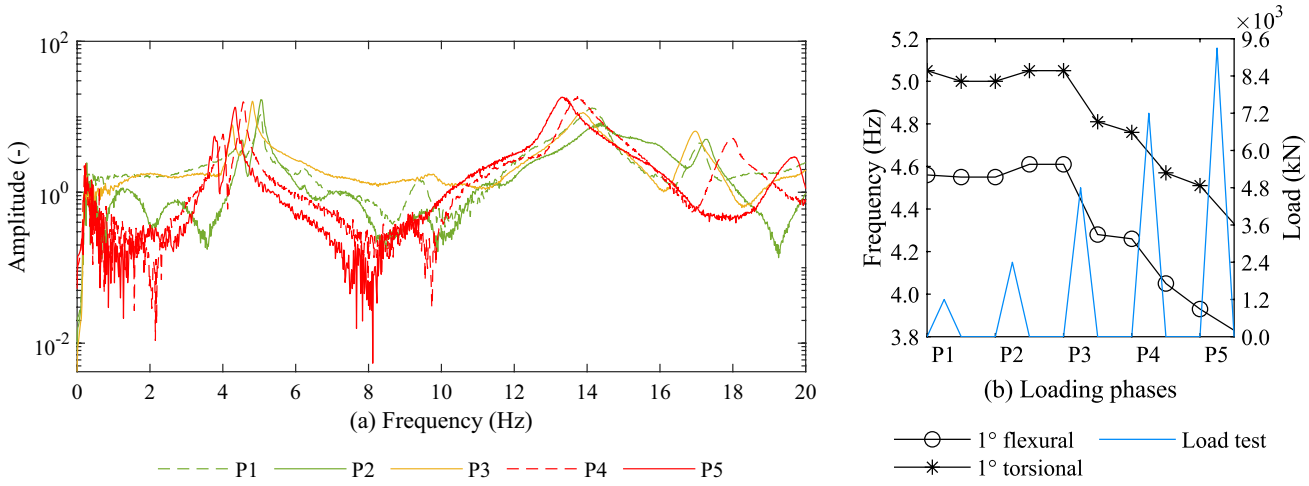

Fig. 17 **a** FRFs from the accelerometer located on the girder T4 under the weight drops before P1 and at the end of each unloading phase. **b** variation of the first two modal frequencies during the load test

4.3.3 Vibrational measurements

We performed an experimental modal analysis [44] with the vibrational measurements recorded after each loading and unloading phase P1–P5. It allowed us to determine the peak frequencies of the span and observe their variation during the test. The vibrational measurements were acquired for 60 s at a sampling frequency of 800 Hz by 15 accelerometers attached solidly to the structure, positioned below the slab: ten vertical axis accelerometers and five horizontal axis accelerometers. We provided an artificial excitation to the structure by dropping a 50 kg weight from a height of 0.50 m.

We dropped the weight always in the same position on the girder T4 at a distance of *L*/4 from the abutment. We repeated the dynamic test before, during, and after each loading and unloading phase. For safety reasons, during phases P4 and P5, we performed the dynamic test at 4800 kN and not at the end of the loading phases. We processed the acquired data with the software Diadem (National Instruments).

Figure 17a shows the frequency response functions (FRFs) obtained from the accelerometer placed under the girder T4 where the weight drops before the loading phase P1 and at the end of each unloading phase (always with the bridge unloaded). It is possible to observe to what extent the peak frequencies change as the damage progresses, while the boundary conditions (mass and constraints) do not change. We focused mainly on frequencies below 10 Hz to control the evolution of the first modes of the span. The two peak frequencies appear as a double peak with closely spaced frequencies, which progressively move towards the lower frequencies as the applied load increases (from P1 to P5) and the damage progresses. The peak frequencies variations of the first two vertical modes (always measured with the bridge unloaded) are summarised in Table 12 and represented in Fig. 17b. They highlight a downward trend before and after each loading phase. The reduction during P3 confirms the change in the girders' stiffness; thus, the change from state I (elastic) to state II (cracked) occurred during P3.

Table 12 Peak frequencies of the first two vertical modes calculated before and after each loading and unloading phase

Phase	Load (kN)	First vertical mode				Second vertical mode			
		Before (0 kN)	Max. load		After (0 kN)	Before (0 kN)	Max. load		After (0 kN)
P1	1200	4.55	3.96		4.63	5.05	4.63		5.00
P2	2400	4.55	3.44		4.61	5.00	4.21		5.05
P3	4800	4.61	2.53		4.28	5.05	3.24		4.81
P4	7200	4.26	2.28[a]	2.13[b]	4.05	4.76	3.07[a]	2.68[b]	4.57
P5	9600	3.93	2.48[a]	2.25[b]	3.83	4.51	3.12[a]	2.83[b]	4.33

[a]During the loading phase at 4800 kN

[b]During the unloading phase at 4800 kN. For P4 and P5, the acquisition at maximum load was performed at 4800 kN for safety reasons

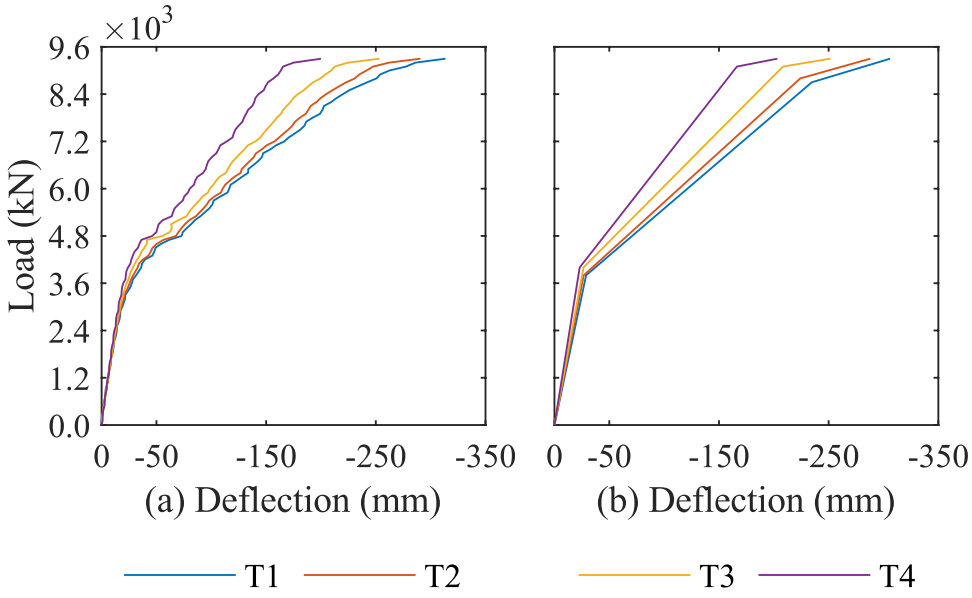

Fig. 18 **a** Envelope of the vertical deflection at the girders' midspan plotted against the load and **b** their trilinear idealised flexural response

Table 13 Stiffness of each girder estimated through their trilinear idealised flexural response

State	T1—k [kN/mm]	T2—k [kN/mm]	T3—k [kN/mm]	T4—k [kN/mm]
I—Elastic	131.71	142.55	151.00	173.83
II—Cracked	23.82	25.32	28.04	35.58
III—Post-failure	8.40	7.84	4.64	5.42

Table 14 Loads corresponding to the change from state I to II and from state II to III of each girder

State change	T1—Load [kN]	T2—Load [kN]	T3—Load [kN]	T4–Load [kN]
I–II	3800	3800	4000	4000
II–III	8700	8800	9100	9100

5 Discussion

5.1 Model prediction vs observed response

In this subsection, we report the girders' predicted and observed vertical deflection, their stiffnesses resulting from the trilinear idealised flexural response, their first-crack load, and ultimate load-carry capacity. Figure 18a shows the envelope of the vertical deflections measured at the midspan of each girder by the monitoring system, while Fig. 18b shows their trilinear idealised flexural response. As explained in Sect. 4.3.1, the girder T1 experienced the greatest deflection, up to 30% more than the others. That is probably due to the highest stiffness of T4, the cross girders' influence on the loads' redistribution, and the different cracks' initiation and propagation among girders. Indeed, all girders have a similar stiffness in state I (elastic) but a visibly different stiffness in state II (cracked). Table 13 reports the stiffness of each girder estimated through their trilinear idealised flexural response, and Table 14 reports the loads corresponding to the changes in structural states.

Figure 19 shows a comparison between the predicted and the observed deflections at the midspan of the girders. The predictions result from hypotheses A, B and C of model ANA1, hypotheses B and C of model ANA2, and hypothesis C of model FEM1 and FEM2. Table 15 reports the stiffness of each girder resulting from the prediction models, and Table 16 reports the loads corresponding to changes in the structural states.

5.2 Errors in the predictions

In this subsection, we analyse whether the observed structural stiffnesses in states I, II, and III, the first-crack loads, and the failure loads align with the predictions, and we quantify the prediction errors. Then, we discuss the rationale and the procedure of the model updating we performed. Table 17 reports the errors in the prediction of stiffnesses, and Table 18 reports the errors in the prediction of loads.

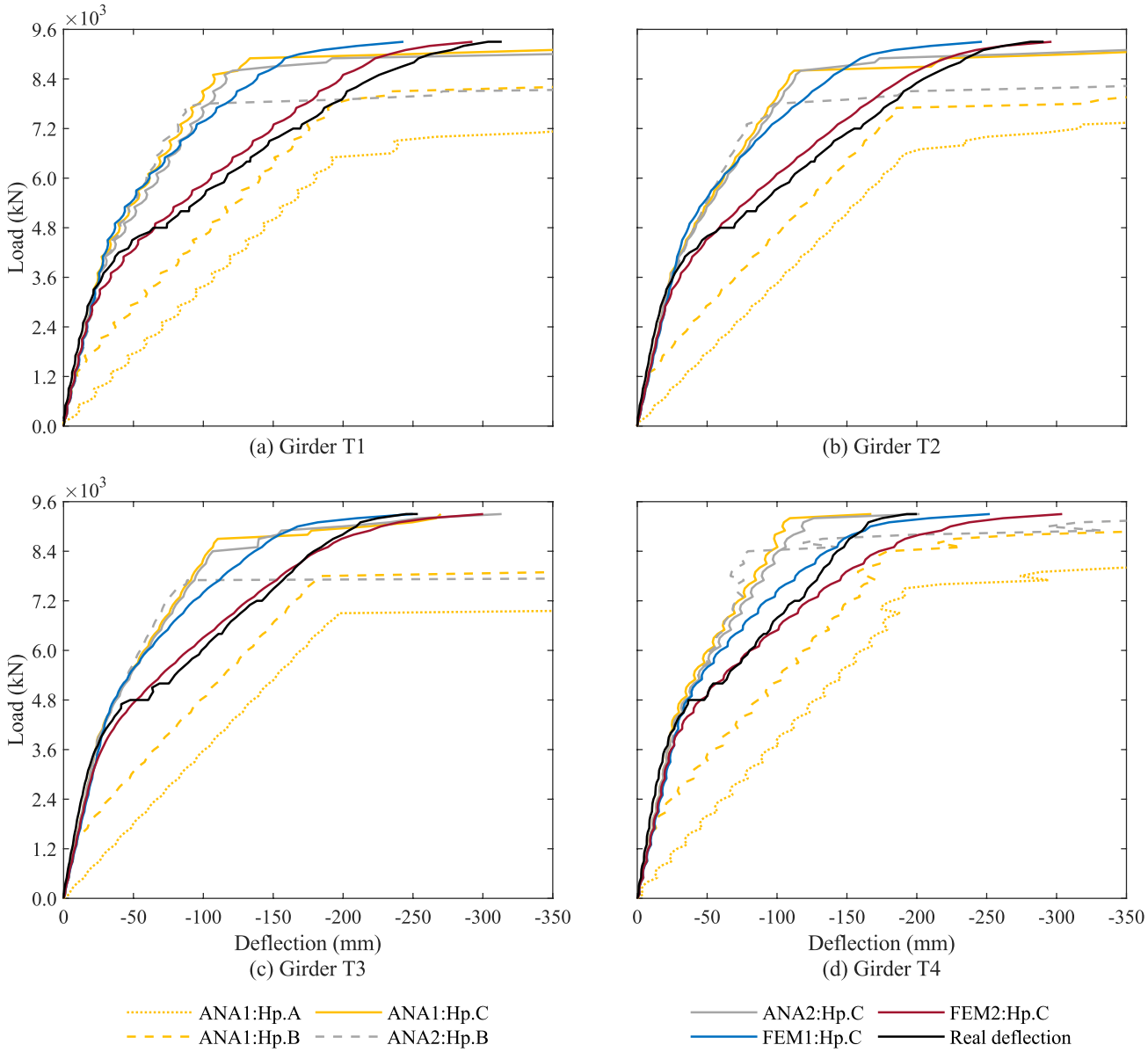

Fig. 19 Comparison between the predicted and the observed deflections at the midspan of girders: **a** T1, **b** T2, **c** T3, and **d** T4

5.2.1 Model ANA1

The predictions of the structural response provided by the model ANA1 result from the hypotheses defined based only on the design documentation and NDTs on material specimens, without any evidence of the actual response of the bridge during the load test. The differences between that prediction and the response measured by the monitoring system raise the following observations:

- Elastic stiffness (slope of state I): the predictions from hypotheses B and C align with the observations.
- Cracked stiffness (slope of state II): the predictions are higher than the observations; predictions resulting from hypothesis B are more likely than from hypotheses A and C.
- Post-failure stiffness (slope of state III): the predictions are slightly lower than the observations.
- First-crack load (change from state I to II): hypothesis C's predictions align with the observation, while hypotheses A and B are very different.

Table 15 Stiffness of each girder predicted by the structural models

k [kN/mm]		Hp. A				Hp. B				Hp. C			
Model	State	T1	T2	T3	T4	T1	T2	T3	T4	T1	T2	T3	T4
ANA1	I	33.06	34.14	35.09	37.32	121.2	140.22	147.2	143.03	144.8	152.72	158.44	166.43
	II	5.68	5.26	0.36	2.3	34.77	35.66	36.41	38.21	48.89	54.78	55.04	56.78
	III	1.53	1.33	2.15	–	1.4	1.82	2.21	2.91	1.27	2.02	3.56	1.72
ANA2	I	–	–	–	–	136.29	141.44	146	150.15	130.96	135.23	132.70	147.55
	II	–	–	–	–	63.24	67.26	66.2	55.91	51.52	53.37	58.82	52.42
	III	–	–	–	–	0.69	1.28	0.97	1.69	2.20	2.15	3.32	2.43
FEM1	I	–	–	–	–	–	–	–	–	133.55	130.70	142.42	160.00
	II	–	–	–	–	–	–	–	–	32.89	30.42	33.57	22.20
	III	–	–	–	–	–	–	–	–	4.71	5.15	3.25	9.06
FEM2	I	–	–	–	–	–	–	–	–	130.00	125.68	133.33	156.32
	II	–	–	–	–	–	–	–	–	25.92	25.63	36.55	27.59
	III	–	–	–	–	–	–	–	–	5.75	4.52	2.25	2.94

Table 16 Loads corresponding to the change in the structural states predicted by the structural models

Load [kN]		Hp. A				Hp. B				Hp. C			
Model	State	T1	T2	T3	T4	T1	T2	T3	T4	T1	T2	T3	T4
ANA1	I–II	6500	6600	6900	7600	1500	1400	1600	2000	4400	4000	4200	4600
	II–III	7000	7400	7000	–	7700	7700	7700	8500	8700	8600	8700	9200
ANA2	I–II	–	–	–	–	3900	3900	3900	4000	3900	3900	3900	4000
	II–III	–	–	–	–	7700	7700	7700	8400	8600	8600	8700	9200
FEM1	I–II	–	–	–	–	–	–	–		4900	4900	4700	4800
	II–III	–	–	–	–	–	–	–	–	8900	8900	9000	9000
FEM2	I–II	–	–	–	–	–	–	–	–	3900	3900	4000	4200
	II–III	–	–	–	–	–	–	–	–	8900	9000	9000	9000

Table 17 Errors in the stiffness prediction

Error in *k* [%]		Hp. A				Hp. B				Hp. C			
Model	State	T1	T2	T3	T4	T1	T2	T3	T4	T1	T2	T3	T4
ANA1	I	− 74.9	− 76.1	− 76.8	− 78.5	− 7.98	− 1.63	− 2.52	− 17.7	9.94	7.13	4.93	− 4.26
	II	− 13.8	− 14.1	− 18.3	− 19.2	8.31	7.25	5.54	1.51	19.0	20.7	17.9	12.2
	III	− 5.22	− 4.57	− 1.7	–	− 5.31	− 4.22	− 1.61	− 1.44	− 5.41	− 4.08	− 0.72	− 2.13
ANA2	I	–	–	–	–	3.48	− 0.78	− 3.31	− 13.6	− 0.57	− 5.14	− 12.1	− 15.1
	II	–	–	–	–	29.9	29.4	25.8	11.7	21.0	19.7	20.4	9.69
	III	–	–	–	–	− 5.85	− 4.60	− 2.43	− 2.15	− 4.71	− 3.99	− 0.88	− 1.72
FEM1	I	–	–	–	–	–	–	–	–	1.40	− 8.31	− 5.68	− 7.96
	II	–	–	–	–	–	–	–	–	6.89	3.57	3.66	− 7.70
	III	–	–	–	–	–	–	–	–	− 2.80	− 1.88	− 0.92	2.10
FEM2	I	–	–	–	–	–	–	–	–	− 1.30	− 11.8	− 11.7	− 10.1
	II	–	–	–	–	–	–	–	–	1.59	0.22	5.64	− 4.60
	III	–	–	–	–	–	–	–	–	− 2.01	− 2.33	− 1.58	− 1.43

Error = (prediction − observation)/(observation of k_I) × 100 [%]

- Failure load (change from state II to III): the predictions from hypotheses A and B are lower than the observations, while hypothesis C seems more likely.

The prediction errors strongly depend on the hypotheses of materials. The main differences are (i) in the elastic stiffness, with error > 70% in hp. A and error < 10% in hp.

Table 18 Errors in the load prediction

Error in load [%]		Hp. A				Hp. B				Hp. C			
Model	State	T1	T2	T3	T4	T1	T2	T3	T4	T1	T2	T3	T4
ANA1	I–II	31.0	31.8	31.8	39.6	− 26.4	− 27.3	− 26.4	− 22.0	6.90	2.27	2.20	6.59
	II–III	− 19.5	− 15.9	− 23.1	–	− 11.5	− 12.5	− 15.4	− 6.59	0.00	− 2.27	− 4.40	1.10
ANA2	I–II	–	–	–	–	1.15	1.14	− 1.10	0.00	1.15	1.14	− 1.10	0.00
	II–III	–	–	–	–	− 11.5	− 12.5	− 15.4	− 7.69	− 1.15	− 2.27	− 4.40	1.10
FEM1	I–II	–	–	–	–	–	–	–	–	12.64	12.50	7.69	8.79
	II–III	–	–	–	–	–	–	–	–	2.30	1.14	− 1.10	− 1.10
FEM2	I–II	–	–	–	–	–	–	–	–	1.15	1.14	0.00	2.20
	II–III	–	–	–	–	–	–	–	–	2.30	2.27	− 1.10	− 1.10

Error = (prediction − observation)/(observation of Load II–III) × 100 [%]

C; and (ii) in the first-crack load, with error > 30% in hp. A, error < 7% in hp. C. The first-crack load is particularly sensitive to the residual stress in prestressing cables; thus, it must be accurately estimated with NDTs.

5.2.2 Model ANA2

We updated the analytical model ANA1 by changing the residual stress of prestressing cables to make the predicted first crack loads as close as possible to the observed ones. Table 5 of Sect. 3.3.2 reports the updated values of residual stress. In addition, we neglected material hypothesis A, since it seemed excessively precautionary.

As a result, the predictions of model ANA2 result from hypotheses defined based on the design documentation, NDTs on material specimens, and a diagnostic load test on the bridge (previously uncracked) carried on until the first crack opens and without any evidence of the cracked stiffness and ultimate capacity. The differences between that prediction and the response measured by the monitoring system raise the following observations:

- Elastic stiffness: predictions are in line with the observation.
- Cracked stiffness: predictions are still higher than the observation; this time, prediction from hp. C is more likely than hp. B.
- Post-failure stiffness: predictions are slightly lower than observations; they do not change while changing the residual stress.
- First-crack load: hypotheses B and C predictions are now almost equivalent to the observations.
- Failure load: predictions do not change while changing the residual stress; therefore, hypothesis C is still more likely than B.

From a load test carried on until the first-crack opening, it is possible to learn the elastic response of the bridge—elastic stiffness and first-crack load—and update the model so that its prediction of elastic response better fits the observation. In particular, we can update the residual stress of prestressing steel, which is difficult to estimate with NDTs and strongly influences the first-crack load of PC girders. However, this load test will crack the structural elements; therefore, it might be unsuitable for an in-service bridge. After the model updating, the prediction error on the first crack load decreased from a mean value of 20% to around 1%. On the other hand, the prediction error on the cracked stiffness changed only slightly, as well as the error in the prediction of the ultimate capacity and the post-failure stiffness; that is because they typically do not change while changing the residual stress.

5.2.3 Model FEM1

To better fit the response of the bridge measured during the entire load test, we developed a finite-element model FEM1 with the hypotheses described in Sect. 3.3.2. As far as the properties of the materials, we considered only hp. C.

The predictions of model FEM1 result from the same hypotheses as ANA2; however, it is a finite-element model with more refined geometry and non-linear stress–strain relations. The differences between that prediction and the response measured by the monitoring system raise the following observations:

- Elastic stiffness: prediction is in line with the observation but slightly lower.
- Cracked stiffness: prediction is closer to the observation than before but still slightly higher.
- Post-failure stiffness: prediction is in line with the observation; the comparison is easier to perform for girder T3

and T4, since they experienced a more extended post-failure response.
- First-crack load: prediction is now higher than observation; a further update of the residual stress of prestressing cables is needed.
- Failure load: prediction is in line with the observation.

The results are similar to those obtained from model ANA2, apart from the first-crack load. The prediction errors increased, because we used the residual stress updated ad hoc to make the prediction of ANA2 fitting better the observed response. However, the updated residual stress value did not bring the same result for the model FEM1. Not surprisingly, the output of a parameter updating process depends strongly on the model; if we change the model, we must update the parameters again to make the new model fit the observation.

5.2.4 Model FEM2

We performed a sensitivity analysis on the parameters of the model FEM1 to better establish their influence on the model prediction and select their values that make the model predictions better fit the observed response during the entire load test. We tested all their possible combinations in a range of $[-10\%, +10\%]$ of their nominal value used in the model FEM1. The results of the sensitivity analysis suggest that:

- Elastic stiffness is strongly influenced by the elastic modulus of the girders' concrete. That aligns with what we expected, given the well-known theory of beams and the constitutive laws of materials. Other parameters do not significantly influence the predicted response in state I.
- Cracked stiffness depends mainly on the residual stress of prestressing cables and slightly on the tensile strength of concrete. According to the theory of prestressed beams, PC girders should not be affected by this parameter once the crack has occurred; however, the first-crack load is affected by the residual stress, affecting the cracked stiffness in turn.
- First-crack load depends on the concrete's tensile strength and the prestressing cables' residual stress. Therefore, we achieved an improvement by decreasing the residual stress, which resulted in a decrease in the predicted first-crack load. This change does not affect the ultimate load. Other parameters do not significantly affect the predicted response in state II.
- Ultimate capacity depends on concrete's tensile and compressive strength, the yield and ultimate tensile strength of prestressing steel, and the ultimate strain of concrete and steel. It does not depend much on the elastic modulus of the concrete and the residual stress of prestressing steel; therefore, its predicted value has never changed much between different models.

As a result, the most influential parameters of the finite-element model of the viaduct are:

- E_c: the elastic modulus of the concrete for structural elements in state I.
- $\sigma_{p,\infty}$: the residual stress of prestressing steel for structural elements in state II.

Table 6 of Sect. 3.3.2 reports the updated values of the prestressing steel's residual stress and the concrete's elastic modulus. We observe that the prestressing cables have lost considerable tension over time and that the loss has been non-uniform between the girders. Indeed, the girder T1 lost around 30% of the initial prestressing tension, the girders T2 and T3 around 20%, and the girder T4 less than 10%.

Looking at Tables 17 and 18, we note a marked improvement in the model predictions from model FEM1 to model FEM2. The elastic, the cracked, and the post-failure predicted response align with the observation, and differences are negligible (error $< 10\%$ for the stiffness, error $< 3\%$ for the load).

From a load test carried on until the bridge's failure, it is possible to learn the bridge's elastic, cracked, and post-failure response, the first crack load of its structural elements, and its ultimate capacity. However, such a load test will collapse the bridge; therefore, it is not unsuitable for an in-service bridge.

The prediction of the structural response becomes more accurate as the load test provides more information to update the structural model. The only difference is between model ANA2 and FEM1, where some quantities are better predicted by ANA2 than FEM1, as explained in Sect. 5.2.3. Figure 20 shows the variation of the prediction

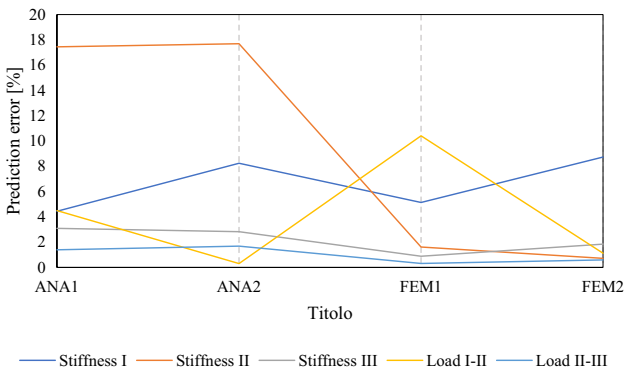

Fig. 20 Differences between model predictions and observed response. Quantities are expressed in % respect to the observed value of the elastic stiffness and ultimate capacity, respectively. Error = abs (observation–prediction)/observation %

errors between the models. Quantities are expressed here in absolute value.

5.3 Load test utility for model updating

This subsection focuses on the question, "What can we learn from a load test?". A load test can provide useful information on the condition state of a bridge. We can use it to update the parameters of a model to improve its prediction of the structure response; however, different load tests provide different information with different impacts on the model updating. We represent different load tests with our five loading phases P1–P5 and different levels of model updating with our four prediction models. We aim to verify whether diagnostic load test of the bridge's elastic response or proof tests with higher loads allow to:

- Discriminate whether the bridge has preexisting concrete cracks or not.
- Identify the opening of the first crack during the load test.
- Estimate the prestressing cables' residual stress.
- Update the structural model to predict the ultimate capacity of the bridge better.

5.3.1 Elastic vs cracked response

The loading phases P1 and P2 tested the elastic response of the bridge, because it had no preexisting cracks, and the resulting bending moments in the girders did not exceed the yield strength of materials. In contrast, the loading phase P3 opened the first cracks in the girders. Finally, the loading phases P4 and P5 tested the cracked response of the bridge, because the bridge experienced the initiation and propagation of cracks during the previous phase, P3.

Green lines in Figs. 12 and 14 of Sect. 4.3.1 (phases P1 and P2) clearly show the linear elastic response of the bridge and point out the absence of preexisting cracks in all girders, since no residual vertical deflections nor longitudinal deformation remains after the unloading of the span. The same result comes from the acoustic emission sensors on girders T2 and T3 and the modal analysis. We did not observe any acoustic emissions from concrete cracks during the loading and unloading phases P1 and P2 (extensive results are in [30]). Moreover, the first flexural and the first torsional frequencies do not change after P1 and P2.

In contrast, the amber lines (phases P3) in Figs. 12 and 14 show a sharp change in the slope due to a change in the girders' response: from state I to state II. The acoustic emissions sensors confirm that (see [30]); they suddenly started recording a high number of high-amplitude and high-strength signals, which identifies the behaviour change of girders T2 and T3. Also, the modal analysis confirms that Fig. 17 shows a reduction of around 0.2 Hz of both the first flexural and the first torsional frequencies after the unloading phase of P3.

Finally, the red dashed lines (phase P4) in Figs. 12 and 14 show a non-linear response starting from the beginning of the loading phase: the stiffness is half of what was observed during phases P1 and P2, and a residual deflection and deformation remains after the unloading of the bridge. Acoustic emission sensors recorded many signals from cracks opening and propagation, as reported in [30, 45], and the modal analysis shows a further reduction of 0.2 Hz after P4.

The prediction of model ANA1, whose parameters we have estimated only based on design documentation and NDTs of material specimens, identified the elastic stiffness with good accuracy: error $< 20\%$ (with hp. B and hp. C).

As a result, regular diagnostic tests up to the design traffic load can effectively discriminate whether a PC bridge has preexisting concrete cracks or not by comparing the observed stiffness with the predicted one. When the observation is slightly different from the prediction (error $< 20\%$), the bridge is likely uncracked; the analyst can update the elastic modulus of concrete to have a more accurate prediction of its elastic response. A regular diagnostic test can also point out whether the opening of the first crack happens during the test and identify precisely the first-crack load.

5.3.2 Residual stress of prestressing cables

We observed that the residual stress of prestressing cables mainly influences the first-crack load, which in turn influences the stiffness in state II. Therefore, a regular diagnostic load test of an uncracked bridge cannot provide useful information to estimate it accurately. For an accurate residual stress estimation, the load test should identify the first-crack load; then, we can identify the updated residual stress by forcing the model prediction to crack at the same load, as we did with models ANA2. However, this procedure might be unsuitable for in-service bridges that must stay uncracked. The residual stress is probably just fine if bridges are still uncracked after 50 years. Moreover, residual stress typically does not influence the ultimate capacity; therefore, its accurate knowledge is generally not mandatory to verify the structural reliability of the bridge.

On the other hand, a diagnostic test up to a higher load than the predicted first-crack load can provide evidence of the cracked stiffness of a cracked bridge without a considerable increase in the damage level. In this case, the first-crack load will not show a marked change in the response as in the uncracked bridge. As a result, the residual stress can be better estimated. The knowledge of the residual stress is more

important for a cracked bridge, since it influences its serviceability (deflection) and durability (cracks' propagation).

5.3.3 Prediction of ultimate capacity

We observed that the ultimate capacity of the bridge depends mainly on the tensile and compressive strength of the concrete, the yield and ultimate tensile strength of prestressing cables, and the ultimate strain of concrete and steel. Therefore, load tests of the elastic response of the bridge do not provide any useful information about the ultimate capacity, nor do load tests that exceed the first-crack load. However, all prediction models with material hypothesis C provide a pretty good estimation of the ultimate capacity, even the model ANA1. The prediction errors are all lower than 5%. Therefore, it seems more important to perform an extensive NDTs' campaign on material specimens to estimate the material properties accurately rather than load tests. A load test to failure is not an option to identify the ultimate capacity of a particular bridge, since it would have to be dismissed after the load test.

Testing a bridge to failure can be particularly informative if that bridge has already been dismissed and is part of an asset that consists of many bridges with similar structural type, age, and deterioration state as the Alveo Vecchio viaduct was. Indeed, the load test described in this paper allowed us to verify that the ultimate moment resistance of the Alveo Vecchio viaduct has been almost four times what the design documentation reported. Most Italian bridges with similar characteristics are likely to have a similar ultimate capacity, or at least they can carry the design traffic load without much distress. However, particular attention should be paid to structures in marine, industrial, and aggressive environments, where the corrosion might induce an accelerated degradation and, consequently, an accelerated reduction of structural capacity and durability.

6 Conclusions

As civil infrastructure ages and the volume of road traffic increases, it is crucial to verify that bridges older than 50 can carry the new traffic loads without distress. Numerical models can predict their operational response to traffic loads and their ultimate capacity with low uncertainties; however, such uncertainties increase as bridges age due to deterioration mechanisms. Non-destructive tests on material specimens increase the knowledge of materials' properties; on-site diagnostic and proof load tests provide different information on the structural health state depending on the load applied during the test.

This paper summarises the research activity performed at the MIMS Infrastructure Safety Test Field setup at the Alveo Vecchio viaduct in Italy. The structure is a decommissioned PC bridge representing 52% of the Italian highway bridges in terms of structural type, age, and deterioration state. We subjected it to a load test performed in five phases with a progressively increasing load up to its failure. We measured its static and dynamic response with an extensive structural health monitoring system during the entire load test. We reported it in this manuscript, along with a detailed description of the design and execution of the test. In addition, we developed an analytical and an FE model of the structure. We progressively updated them based on non-destructive tests of material specimens and monitoring system results acquired during the test. This paper compares the structure's observed response during the load test with its predicted response by structural models. A detailed discussion follows. First, the paper discusses what engineers can observe and learn from a load test as the load progressively increases (e.g., stiffness, first-crack load, and ultimate capacity). Then, it identifies the model parameters that influence the response prediction the most. Finally, it verifies whether a diagnostic load test up to the design traffic load allows verifying whether: (i) the structural response is elastic during the entire load test; (ii) the bridge cracks during the load test; (iii) the bridge was already cracked before the load test. The main results are:

1. The elastic modulus of concrete was the parameter that influenced the elastic stiffness the most; the residual stress of prestressing cables was the parameter that influenced the first-crack load and the crack stiffness the most.
2. The ultimate capacity seemed to depend mainly on the tensile and compressive strength of the concrete, the yield and ultimate tensile strength of prestressing cables, and the ultimate strain of concrete and steel.
3. Both analytical and FE models based only on the design documentation and NDTs of material specimens predicted the girders' elastic stiffness with an error of $<20\%$ and the ultimate capacity with an error of $<5\%$ when NDTs carefully estimated the material properties.
4. The load test up to the design traffic load allowed recognising whether the PC bridge had preexisting concrete cracks by comparing the observed stiffness with the predicted one.
5. The load test effectively pointed out whether the opening of the first crack happened or not during the loading phases, showing a sharp change in the slope of the load–deflection graph. The first-crack load was clearly detectable.
6. When the PC bridge had no preexisted cracks, the load test up to the design traffic load did not provide useful information to estimate the residual stress of prestressing cables. To have them, we had to crack the girders, which

is not an option for in-service bridges. To estimate the residual stress, performing NDTs of material specimens is preferable.

7. When the PC bridge was already cracked, the load test with a higher load than the predicted first-crack load did not show a marked change in the observed response as in the uncracked bridge. That allowed measuring the cracked stiffness without a considerable increase in the damage level.
8. Load tests of the elastic response did not provide information about the ultimate capacity, nor did load tests that exceeded the first-crack load. The last load test (which collapsed the bridge) did it; however, a load test to failure is not an option for in-service bridges, since they would have to be dismissed after the load test.
9. A load test up to a bridge failure can be particularly informative if that bridge has already been dismissed and is part of an asset that consists of many bridges with similar structural type, age, and deterioration as the Alveo Vecchio viaduct was. The load test described in this paper allowed us to verify that the ultimate moment resistance of the Alveo Vecchio viaduct was almost four times what the design documentation reported.

Acknowledgements The authors wish to thank all the people who collaborated to the success of this project, including P. Migliorino (Italian Ministry of Sustainable Infrastructures and Mobility); A. Selleri, A. Marchiondelli, M. Cicolani, M. Conte, L. Tripoli, P. Anfosso, M. Di Napoli, M. Perna, and D. Sena (Autostrade per l'Italia SpA); G. Ascari (Akron); F. Sandrin (Vernazza Autogru).

Funding Open access funding provided by Università degli Studi di Trento within the CRUI-CARE Agreement. The work presented in this paper is part of a research collaboration among the University of Trento, the Italian Ministry of Infrastructures and Transport, and Autostrade per l'Italia SpA. This research has been supported also by MIUR PON RI 2014-2020 Program (project MITIGO, ARS01_00964), Fondazione CARITRO Cassa di Risparmio di Trento e Rovereto (Grant number 2021.0224), Consorzio ReLUIS (Project ReLUIS Ponti 2021-2022 'Implementation of provisions of DM 578/2020').

References

1. ASCE American Society of Civil Engineers (2021) Report card for America's infrastructure, 2021. [Online]. https://infrastructurereportcard.org/. Accessed 2021
2. Ministry of Land, Infrastructure, Transport and Tourism of Japan (2019) White paper on land, infrastructure, transport, and tourism in Japan in 2019. [Online]. https://www.mlit.go.jp/en/statistics/white-paper-mlit-2019.html. Accessed 2021
3. Ministry of Land, Infrastructure, Transport and Tourism of Japan (2020) Summary of white paper on land, infrastructure, transport, and tourism in Japan in 2020. [Online]. https://www.mlit.go.jp/en/statistics/white-paper-mlit-index.html. Consultato il giorno 2021
4. AASHTO LRFD bridge design specifications, 8th edition (2017) Washington, D.C.: American Association of State Highway and Transportation Officials
5. European Committee for Standardization (2005) EN 1992-2 Eurocode 2—design of concrete structures—concrete bridges—design and detailing rules. CEN, Brussels
6. Italian Ministry of Infrastructure and Transport (2018) Norme Tecniche per le Costruzioni D.M. 17/01/2018. [Online]. http://www.gazzettaufficiale.it/eli/id/2008/02/04/08A00368/sg. Accessed 2021
7. Bencivenga P, Buratti G, Cosentino A, Matteis GD, Morelli F, Salvatore W, Zizi M (2022) Evolution of design traffic loads for Italian road bridges, pp 1351–1358. https://doi.org/10.1007/978-3-030-91877-4_154
8. U.S. Department of Transportation Federal Highway Administration (2015) Compilation of existing state truck size and weight limit laws. [Online]. https://ops.fhwa.dot.gov/freight/policy/rpt_congress/truck_sw_laws/index.htm#back. Accessed 2021
9. UK Department for Transport, Driving Standards Agency (2017) The official highway code 2007 edition. The Stationery Office
10. Italian Ministry of Infrastructure and Transport (2021) Codice della strada. [Online]. https://www.aci.it/i-servizi/normative/codice-della-strada.html. Accessed 2021
11. Frangopol DM (2007) Maintenance and management of civil infrastructure based on condition, safety, optimization, and life-cycle cost. Struct Infrastruct Eng 3(1):29–41
12. Calvi GM, Moratti M, O'Reilly GJ, Scattarreggia N (2019) Once upon a time in Italy: the tale of the Morandi. Struct Eng Int 29(2):198–217
13. Deng L, Wang W, Yu Y (2016) State-of-the-art review on the causes and mechanisms of bridge collapse. J Perform Constr Facil. https://doi.org/10.1061/(ASCE)CF.1943-5509.0000731
14. Caspani VF, Tonelli D, Poli F, Zonta D (2022) Designing a structural health monitoring system accounting for temperature compensation. Infrastructures. https://doi.org/10.3390/infrastructures7010005
15. Quqa S, Giordano PF, Limongelli MP, Landi L, Diotallevi PP (2021) Clump interpolation error for the identification of damage on board decentralized sensing systems. Smart Struct Syst 27(2):351–363
16. Lantsoght EOL, van der Veen C, de Boer A, Hordijk DA (2017) State-of-the-art on load testing of concrete bridges. Eng Struct 150:231–241
17. Bagge N, Plos M, Popescu C (2019) A multi-level strategy for successively improved structural analysis of existing concrete bridges: examination using a prestressed concrete bridge tested to failure. Struct Infrastruct Eng 15(1):27–53
18. Gómez JD, Casas JR (2008) Assessment of bridge capacity through proof load testing. In: Biondini F, Frangopol D (eds) Life-cycle civil engineering. CRC Press, Boca Raton, pp 579–584. https://doi.org/10.1201/9780203885307-92

19. Alampalli S, Frangopol DM, Grimson J, Halling MW, Kosnik DE, Lantsoght EOL, Yang D, Zhou YE (2021) Bridge load testing: state-of-the-practice. J Bridg Eng. https://doi.org/10.1061/(ASCE)BE.1943-5592.0001678
20. Pressley JS, Candy CCE, Walton BL, Sanjayan JG (2004) Destructive load testing of Bridge No. 1049—analyses, predictions and testing. In: Bridges another dimension. Proceedings of the fifth Austroads bridge conference, Sydney, NSW, Australia
21. Burdette EG, Goodpasture DW (1974) Test to failure of a prestressed concrete bridge. PCI J 19(3):92–103
22. Bagge N, Popescu C, Elfgren L (2017) Failure tests on concrete bridges: have we learnt the lessons? Struct Infrastruct Eng 14(3):292–319
23. Cai SC, Shahawy M (2004) Predicted and measured performance of prestressed concrete bridges. J Bridg Eng 9(1):4–13
24. Papé TM, Melchers RE (2011) The effects of corrosion on 45-year-old pre-stressed concrete bridge beams. Struct Infrastruct Eng 7(1–2):101–108
25. SPEA (1966) Relazione di Calcolo Viadotto Alveo Vecchio alla progr. 39 + 364.21, Opera N*14
26. Italian Govenment (2018) Decreto-Legge 28 settembre 2018, n.109. Gazzetta ufficiale della Repubblica Italiana
27. Ministero delle Infrastrutture e dei Trasporti; Consiglio Superiore dei Lavori Pubblici (2020) Linee Guida Per La Classificazione E Gestione Del Rischio, La Valutazione Della Sicurezza Ed Il Monitoraggio Dei Ponti Esistenti
28. Zonta D, Zandonini R, Bortot F (2007) A reliability-based bridge management concept. Struct Infrastruct Eng 3(3):215–235
29. Mirzaei Z, Adey BT, Klatter L, Kong JS (2012) Overview of existing Bridge Management Systems - Report by the IABMAS Bridge Management Committee. https://www.research-collection.ethz.ch:443/handle/20.500.11850/62546
30. Tonelli D, Luchetta M, Rossi F, Migliorino P, Zonta D (2020) Structural health monitoring based on acoustic emissions: validation on a prestressed concrete bridge tested to failure. Sensors 20(24):1–20. https://doi.org/10.3390/s20247272
31. Brighenti F, Possidente L, Zonta D (2022) Algorithm to estimate the capacity reserve of existing masonry arch railway bridges. Appl Sci 12(2):756
32. Italian Ministry of Public Works (1962) Ministerial circular n. 384 of 14/02/1962—rules related to loads for the calculation of road bridges, Rome
33. Pietrangeli MP (2001) Progettazione e costruzione di ponti. Casa Editrice Ambrosiana, Milano
34. Passaro A (1966) Relazione di calcolo, Viadotto Alveo Vecchio. Report Autostrade - Concessioni e Costruzioni Autostrade S.p.A.
35. European Committee for Standardization (2010) ISO 15630-1:2010 Steel for the reinforcement and prestressing of concrete—test methods—part 1: reinforcing bars, wire rod and wire. CEN, Brussels
36. European Committee for Standardization (2005) EN 1992-1-1 Eurocode 2: design of concrete structures—part 1-1: general rules and rules for buildings. CEN, Brussels
37. Pacific Earthquake Engineering Research (2006) OpenSees. [Online]. https://opensees.berkeley.edu/. Accessed 2021
38. Mazzoni S, McKenna F, Scott MH, Fenves GL (2006) OpenSees command language manual. [Online]. https://opensees.berkeley.edu/OpenSees/manuals/usermanual/OpenSeesCommandLanguageManualJune2006.pdf. Accessed 2020
39. Italian National Unification (2016) UNI/TR 11634:2016 guidelines for structural health monitoring. UNI, Rome
40. Tonelli D, Cappello C, Zonta D (2021) Performance-based design of structural health monitoring systems. In: EWSHM 2020, LNCE proceedings, Palermo, Italy
41. Bado M, Casas J (2021) A review of recent distributed optical fiber sensors applications for civil engineering structural health monitoring. Sensors 21(5):1–83
42. Possidente L, Weiss A, de Silva D, Pustorino S, Nigro E, Tondini N (2021) Fire safety engineering principles applied to a multi-storey steel building. Struct Build 174(9):725–738
43. Bishop CM (2006) Pattern recognition and machine learning. Springer, Berlin
44. Ewins DJ (2000) Modal testing: theory, practice and application. Wiley, Hoboken
45. Tonelli D, Rossi F, Luchetta M, Zonta D, Migliorino P, Selleri A, Valeri E, Marchiondelli A, Ascari G (2021) Acoustic emission monitoring of prestressed concrete bridges: Differences before and after the first-crack opening, pp 389–402. https://doi.org/10.1007/978-3-030-74258-4_26